Maximizing CRISPRi efficacy and accessibility with dual-sgRNA libraries and optimal effectors

Joseph M. Replogle[1-4,†], Jessica L. Bonnar[2-4,†], Angela N. Pogson[2-4,†,‡], Christina R. Liem[2,‡], Nolan K. Maier[5], Yufang Ding[5], Baylee J. Russell[5], Xingren Wang[5], Kun Leng[1,6], Alina Guna[2,4], Thomas M. Norman[2,‡], Ryan A. Pak[2,‡], Daniel M. Ramos[7,8], Michael E. Ward[9], Luke A. Gilbert[2,10,11], Martin Kampmann[6,12], Jonathan S. Weissman[2-4,13,14,*], Marco Jost[2,5,*]

[1]Medical Scientist Training Program, University of California, San Francisco, San Francisco, CA 94158, USA

[2]Department of Cellular and Molecular Pharmacology, University of California, San Francisco, San Francisco, CA 94158, USA

[3]Howard Hughes Medical Institute, Massachusetts Institute of Technology, Cambridge, MA 02142, USA

[4]Whitehead Institute for Biomedical Research, Cambridge, MA 02142, USA

[5]Department of Microbiology, Harvard Medical School, Boston, MA 02115, USA

[6]Institute for Neurodegenerative Disease, University of California, San Francisco, San Francisco, CA 94158, USA

[7]Center for Alzheimer's Disease and Related Dementias, National Institutes of Health, Bethesda, MD 20892, USA

[8]National Institute on Aging, National Institutes of Health, Bethesda, MD 20892, USA

[9]National Institute of Neurological Disorders and Stroke, NIH, Bethesda, MD 20892, USA

[10]Department of Urology and Helen Diller Family Comprehensive Cancer Center, University of California, San Francisco, CA 94158, USA

[11]Arc Institute, Palo Alto, CA, 94304, USA

[12]Department of Biochemistry and Biophysics, University of California, San Francisco, San Francisco, CA 94158, USA

[13]Department of Biology, Massachusetts Institute of Technology, Cambridge, MA 02142, USA

[14]David H. Koch Institute for Integrative Cancer Research, Massachusetts Institute of Technology, Cambridge, MA 02142, USA

32 †Co-first authors
33 *Address correspondence to: J.S.W. (weissman@wi.mit.edu); M.J.
34 (marco_jost@hms.harvard.edu)
35
36 ‡Present Addresses:
37 Angela N. Pogson: Department of Developmental Biology, Stanford University School of
38 Medicine, Stanford, CA 94305, USA
39 Christina R. Liem: Division of Biological Sciences, Section of Cell and Developmental Biology,
40 University of California San Diego, La Jolla, CA 92093, USA
41 Ryan A. Pak: Department of Neuroscience, Scripps Research, La Jolla, CA 92037, USA
42 Thomas M. Norman: Computational & Systems Biology Program, Sloan Kettering Institute,
43 Memorial Sloan Kettering Cancer Center, New York, NY 10065, USA
44
45

Abstract

CRISPR interference (CRISPRi) enables programmable, reversible, and titratable repression of gene expression (knockdown) in mammalian cells. Initial CRISPRi-mediated genetic screens have showcased the potential to address basic questions in cell biology, genetics, and biotechnology, but wider deployment of CRISPRi screening has been constrained by the large size of single guide RNA (sgRNA) libraries and challenges in generating cell models with consistent CRISPRi-mediated knockdown. Here, we present next-generation CRISPRi sgRNA libraries and effector expression constructs that enable strong and consistent knockdown across mammalian cell models. First, we combine empirical sgRNA selection with a dual-sgRNA library design to generate an ultra-compact (1-3 elements per gene), highly active CRISPRi sgRNA library. Next, we rigorously compare CRISPRi effectors to show that the recently published Zim3-dCas9 provides the best balance between strong on-target knockdown and minimal nonspecific effects on cell growth or the transcriptome. Finally, we engineer a suite of cell lines with stable expression of Zim3-dCas9 and robust on-target knockdown. Our results and publicly available reagents establish best practices for CRISPRi genetic screening.

63 **Introduction**

64 CRISPR interference (CRISPRi) enables programmable repression of gene expression with
65 broad applications in genome engineering, genetic screening, and cell biology (Doench, 2018).
66 In mammalian cells, CRISPRi requires two components: (i) an effector protein of catalytically
67 dead Cas9 (dCas9) fused to one or more transcription repressor domains, which recruits
68 endogenous epigenetic modulators to the genome, and (ii) a single guide RNA (sgRNA), which
69 directs the effector protein to target DNA (Gilbert et al., 2013). When the sgRNA is targeted to a
70 gene promoter, CRISPRi leads to repressive epigenome editing and knockdown of the gene
71 (Gilbert et al., 2014; Horlbeck et al., 2016a, 2016b).

72 Several features distinguish CRISPRi from Cas9 nuclease-mediated DNA cutting, the
73 major alternative CRISPR/Cas-based approach for loss-of-function genetic studies: i) Unlike
74 Cas9, CRISPRi does not rely on introduction of double-stranded DNA breaks and therefore does
75 not cause genomic rearrangements (Kosicki et al., 2018) and DNA damage-associated toxicity
76 (Meyers et al., 2017), which may be especially limiting in primary and stem cells (Bowden et al.,
77 2020; Haapaniemi et al., 2018; Ihry et al., 2018). ii) CRISPRi tends to confer more homogeneous
78 loss of gene function compared to Cas9, which often generates subpopulations of cells bearing
79 active in-frame indels (Smits et al., 2019). iii) CRISPRi is reversible and thus affords temporal
80 control over gene expression levels (Gilbert et al., 2014; Mandegar et al., 2016). iv) CRISPRi
81 enables titration of gene expression, which for example allows for partial depletion of genes
82 essential for cell growth and interrogation of the resulting phenotypes (Bosch et al., 2021;
83 Hawkins et al., 2020; Jost et al., 2020). v) In turn, one can directly measure the extent of on-
84 target knockdown as well as the corresponding responses in individual cells, for example using
85 single-cell RNA-seq (Perturb-seq), allowing for evaluation of the extent and potential biological
86 significance of cell-to-cell heterogeneity. vi) CRISPRi enables loss-of-function studies for non-
87 coding RNAs, which are difficult to inactivate or repress through CRISPR cutting and the
88 introduction of indels as they are insensitive to frame-shifting mutations (Liu et al., 2017).

89 Like other CRISPR approaches, CRISPRi has been paired with large-scale sgRNA
90 libraries to conduct systematic genetic screens. Such screens have been deployed to identify
91 essential protein-coding and non-coding genes (Gilbert et al., 2014; Haswell et al., 2021;
92 Horlbeck et al., 2016a; Liu et al., 2017; Raffeiner et al., 2020), to map the targets of regulatory
93 elements (Fulco et al., 2019, 2016; Gasperini et al., 2019; Kearns et al., 2015; Klann et al., 2017;

94 Thakore et al., 2015), to identify regulators of cellular signaling and metabolism (Coukos et al.,
95 2021; Liang et al., 2020; Luteijn et al., 2019; Semesta et al., 2020), to uncover stress response
96 pathways in stem cell-derived neurons (Tian et al., 2021, 2019), to uncover regulators of disease-
97 associated states in microglia and astrocytes (Dräger et al., 2022; Leng et al., 2022), to decode
98 regulators of cytokine production in primary human T-cells (Schmidt et al., 2022), to define
99 mechanisms of action of bioactive small molecules (Jost et al., 2017; Morgens et al., 2019; Sage
100 et al., 2017), to identify synthetic-lethal genetic interactions in cancer cells (Du et al., 2017;
101 Horlbeck et al., 2018), and to identify genetic determinants of complex transcriptional responses
102 using RNA-seq readouts (Perturb-seq) (Adamson et al., 2016; Replogle et al., 2022, 2020; Tian
103 et al., 2021, 2019), among others.

104 Despite these successes, two technical factors have limited wider adoption of CRISPRi.
105 First, CRISPRi screening is constrained by the large size of sgRNA libraries. Previous machine
106 learning efforts yielded guide design rules which substantially increased the activity of sgRNA
107 libraries (Horlbeck et al., 2016a; Sanson et al., 2018). Nonetheless, commonly used libraries
108 (e.g., Dolcetto, CRISPRi v2) target each gene with three or more sgRNAs to decrease false
109 negative results in screens. The development of a more compact, highly active sgRNA library
110 would enable CRISPRi screens in new cell types and for more complex phenotypes, especially
111 when cost, time, and/or cell numbers are limiting. Second, there is no clear consensus guiding
112 the use of the different reported CRISPRi effector proteins, complicating the generation of
113 CRISPRi cell models (Alerasool et al., 2020; Carleton et al., 2017; Gilbert et al., 2014; Yeo et
114 al., 2018).

115 Here we present a suite of tools to enable high-quality CRISPRi genetic screening in a
116 broad range of cell models. Based on empirical data aggregated from 126 screens, we design and
117 validate an ultra-compact, highly active CRISPRi library in which each gene is targeted by a
118 single library element encoding a dual sgRNA cassette. Next, we comprehensively compare
119 published CRISPRi effector proteins based on their on-target efficacy and non-specific effects on
120 transcription and cell proliferation. We find that the recently published Zim3-dCas9 provides the
121 best balance between strong on-target knockdown and minimal nonspecific effects. Finally, we
122 generate K562, RPE1, Jurkat, HT29, HuTu-80, and HepG2 cell lines engineered to stably
123 express Zim3-dCas9 and demonstrate robust on-target knockdown across these cell lines. Our
124 results and reagents establish best practices for CRISPRi genetic screening.

125

126 **Results**

127 *Comparison of single and dual sgRNA CRISPRi libraries for genetic screening*

128 A critical mediator of the potential applications of CRISPRi screening is the on-target efficacy
129 and size of the sgRNA library. In recent work, we found that targeting individual genes with
130 dual-sgRNA constructs substantially improved CRISPRi-mediated gene knockdown (Replogle et
131 al., 2020). Building on this result, we asked whether a dual-sgRNA strategy could be used to
132 generate an ultra-compact, genome-wide CRISPRi library.

133 To assess the potential utility of dual sgRNA libraries in systematic genetic screens, we
134 began by cloning two pilot libraries for comparison: (i) one targeting each human gene with two
135 distinct sgRNAs expressed from a tandem sgRNA cassette (dual sgRNA) and (ii) one targeting
136 each human gene by only the single best sgRNA (see *Methods*; Table S1; Supplementary Note
137 1). We also optimized a protocol to amplify and sequence dual-sgRNA cassettes from lentivirally
138 integrated genomic DNA (see *Methods*; Supplementary Note 2). Next, we compared the
139 performance of our single- and dual-sgRNA libraries in a genome-wide growth screen (Figure
140 1A). We transduced K562 cells stably expressing dCas9-KRAB(Kox1) with our libraries, used
141 puromycin to select for cells with lentiviral integration, and harvested cells at day 8 (T_0) and day
142 20 (T_{final}) post-transduction. We amplified sgRNA cassettes from extracted genomic DNA,
143 sequenced to quantify sgRNA abundance in the two populations, and calculated growth
144 phenotypes for each library element by comparing changes in abundance between T_0 and T_{final}
145 (Figure 1C, Table S2). The growth phenotypes produced by the single- and dual-sgRNA libraries
146 were well-correlated with previously published CRISPRi growth screens using 5 sgRNAs per
147 gene (single sgRNA r = 0.82; dual sgRNA r = 0.83; Figure S1A-C) and produced near-perfect
148 recall of essential genes (Figure S1D) (AUC>0.98 for both single- and dual-sgRNA libraries).
149 Yet, for essential genes previously identified by the Cancer Dependency Map (DepMap) (Behan
150 et al., 2019; Tsherniak et al., 2017), the dual-sgRNA library produced significantly stronger
151 growth phenotypes (mean 29% decrease in the growth rate [γ]) than the single-sgRNA library (n
152 = 2,005 genes; single-sgRNA mean $\gamma = -0.20$; dual-sgRNA mean $\gamma = -0.26$; Mann Whitney p-
153 value = $6 \cdot 10^{-15}$; Figure 1C, 1D), suggesting that the dual-sgRNA library confers stronger
154 depletion of target genes.

155 A well-recognized challenge for the use of dual-sgRNA libraries is that the lentiviral
156 reverse transcriptase can undergo template switching between the two copies of the lentiviral
157 genome packaged into each capsid (Adamson et al., 2018, 2016; Feldman et al., 2018; Hill et al.,
158 2018; Horlbeck et al., 2018; Xie et al., 2018). These two copies generally bear two different
159 sgRNA pairs in a pooled dual-sgRNA library, such that template switching can produce a
160 recombined element with sgRNAs targeting different genes. Our sequencing strategy allowed us
161 to directly identify such recombined elements (Figure 1B), which occurred with a frequency of
162 29.4% across replicates, consistent with prior reports (Horlbeck et al., 2018; Replogle et al.,
163 2020). In our downstream analyses, we exclude all recombined elements such that they do not
164 impact phenotypes, although in principle these recombined elements could be used to assess
165 independent effects of the two sgRNAs targeting each gene.
166
167 *Design and validation of ultra-compact, dual sgRNA CRISPRi libraries*
168 Having validated the performance of dual-sgRNA libraries in a systematic genetic screen, we
169 sought to optimize the activity and utility of dual-sgRNA CRISPRi libraries (Figure 1E). To
170 optimize sgRNA selection for each gene, we aggregated empirical sgRNA activity data from 126
171 CRISPRi genetic screens (Table S3) and implemented a three-tiered selection system. First, for
172 genes that are essential in K562 cells, we ranked sgRNAs by growth phenotype. Second, for
173 genes that produced a significant phenotype in one of our previous CRISPRi screens, we ranked
174 sgRNAs by relative *z*-scored phenotype averaged across screens in which the target gene was
175 identified as a hit. Finally, for genes without any empirical effect in a prior screen, we ranked
176 sgRNAs according to predicted activities from the hCRISPRi v2.1 algorithm (see *Methods*)
177 (Horlbeck et al., 2016a). To allow users to select the library size suitable to their application, we
178 cloned sublibraries of the best single element (guide ranked 1+2; referred to as
179 hCRISPRi_dual_1_2), the second best element (guides ranked 3+4; referred to as
180 hCRISPRi_dual_3_4), or the third best element (guides ranked 5+6; referred to as
181 hCRISPRi_dual_5_6) (Table S4).
182 Further examination of the phenotypes from our screens revealed that a small number of
183 elements produced discordant effects between screens, which may arise from bottlenecking or
184 amplification bias (Figure S1A-C). For libraries with multiple elements targeting each gene, such
185 discordant effects can often be mitigated by comparing phenotypes across elements, but this

186 option is not available with single-element libraries. In previously reported CRISPR cutting
187 libraries, incorporation of barcodes into the sgRNA cassette enabled marking and tracing
188 populations of cells derived from individual lentiviral integrations, which allowed for detection
189 of bottlenecking events and amplification bias and thereby improved screen sensitivity and
190 robustness (Michlits et al., 2017; Zhu et al., 2019). Building on these results, we incorporated a
191 set of 215 8-nucleotide barcodes, which we term Integration Barcodes (IBCs), in the tandem
192 sgRNA cassette of our final hCRISPRi_dual_1_2, hCRISPRi_dual_3_4, and
193 hCRISPRi_dual_5_6 libraries (Methods, Table S5). We then optimized a sequencing strategy for
194 simultaneously sequencing the two sgRNAs, the IBC, and a sample index on Illumina
195 sequencers (Figure 1B, Supplementary Note 2).
196 Finally, we sought to test our optimized dual-sgRNA library side-by-side with the
197 recently reported Dolcetto CRISPRi library, which was designed with a differently prioritized
198 sgRNA selection algorithm and uses single-sgRNAs (Sanson et al., 2018). We used direct
199 capture Perturb-seq (Replogle et al., 2020), pooled CRISPR screens with single-cell RNA-seq
200 readout, to measure the on-target knockdown mediated by the top three elements in our dual
201 sgRNA library (guides 1+2, guides 3+4, or guides 5+6) or the three Dolcetto Set A sgRNAs for
202 128 randomly selected genes that are expressed in K562 cells (Table S6). Our dual-sgRNA
203 library significantly outperformed the Dolcetto library, as quantified by the average knockdown
204 (dual-sgRNA median knockdown 82%; Dolcetto median knockdown 65%; Mann Whitney *p*-
205 value = $2.4 \cdot 10^{-7}$) as well as the strongest knockdown per gene (dual-sgRNA median
206 knockdown 90%; Dolcetto median knockdown 87%; Mann Whitney *p*-value = $2 \cdot 10^{-4}$; Figure
207 1F). Indeed, the top-ranked element of our dual-sgRNA library (guides 1+2) alone produced
208 comparable knockdown to the best of all three Dolcetto sgRNAs (dual sgRNA element 1+2
209 median knockdown 86%; best Dolcetto sgRNA median knockdown 87%; Mann Whitney *p*-
210 value = 0.43) (Figure 1G). We note that an analogous dual-sgRNA approach may improve
211 knockdown for the Dolcetto library. Nonetheless, from these data we conclude that our dual-
212 sgRNA library improves on-target knockdown compared to gold-standard CRISPRi libraries.
213
214 *Design of CRISPRi effector expression constructs for systematic comparisons*
215 We next sought to compare different CRISPRi effectors, with the goal of identifying an effector
216 with strong activity and minimal non-specific effects on global transcription and cell growth. We

217 selected four repressor domains that had been described to mediate strong and specific
218 knockdown in dCas9 fusions: 1) the KRAB domain from KOX1 (*ZNF10*), which was used in the
219 original conception of CRISPRi (Gilbert et al., 2013); 2) the KRAB domain from ZIM3, which
220 was recently reported to mediate stronger knockdown than KRAB(KOX1) (Alerasool et al.,
221 2020); 3) the SIN3A interacting domain of MAD1 (SID4x) (Carleton et al., 2017); and 4) the
222 transcription repression domain of MeCP2 (Yeo et al., 2018).
223 To enable direct comparisons, we embedded each effector in a standardized lentiviral
224 expression construct (Figure 2A, Table S7). Briefly, in this construct, expression is driven by a
225 spleen focus-forming virus (SFFV) promoter, with an upstream ubiquitous chromatin opening
226 element (UCOE) to minimize silencing, internal nuclear localization signals (NLSs) and an
227 internal HA tag, a GFP marker linked at the C-terminus via a P2A ribosomal skipping sequence
228 to allow for stable cell line generation by FACS, and a Woodchuck Hepatitis Virus post-
229 transcriptional regulatory element (WPRE) in the 3′ UTR to increase mRNA stability. Where
230 necessary, we included linker sequences derived from the functionally innocuous XTEN domain
231 (Schellenberger et al., 2009) to minimize proteolytic cleavage between dCas9 and fused
232 repressor domains. We attempted to maximize the activity for each repressor domain based on
233 our previous data and data in the literature, although we note that our evaluation is not
234 exhaustive. The final designs of the four effector expression constructs are depicted in Figure S2,
235 with further rationale in the Methods section. We then compared the four effectors with regards
236 to two key criteria: on-target activity and absence of non-specific effects on cell viability and
237 gene expression.
238
239 *CRISPRi effectors containing SID or MeCP2 domains have non-specific effects on cell viability*
240 *and gene expression*
241 The repressor domain of each CRISPRi effector is a transcription factor domain whose
242 overexpression has the potential to cause non-specific (i.e., not mediated by dCas9 targeting) and
243 potentially detrimental effects on transcription or cell proliferation. To test for effects on
244 proliferation, we generated K562 cell lines stably expressing each effector by lentiviral
245 transduction followed by FACS (Figure 2B) and then quantified the effect of each effector on
246 cell proliferation using an internally normalized competitive growth assay. We mixed cells
247 bearing each effector ~1:1 with cells expressing mCherry and quantified growth defects of

248 effector-expressing cells by measuring the ratio of mCherry-negative to mCherry-positive cells
249 over time by flow cytometry. We used mCherry-expressing cells as a reference population
250 instead of parental, GFP-negative cells because some of the effector-expressing cells convert to
251 GFP-negative over time due to silencing, which is difficult to separate from true dropout of
252 effector-expressing cells due to growth defects. Over 19 days, cells expressing dCas9 only,
253 dCas9-Kox1, or Zim3-dCas9 proliferated at the same rate as cells expressing GFP only or non-
254 transduced control cells, suggesting that expression of these effectors is not toxic over this time
255 span (Figure 2C). By contrast, cells expressing SID-dCas9-Kox1 had a strong growth defect
256 (~6% per day), and cells expressing dCas9-Kox1-MeCP2 had a mild growth defect (~1% per
257 day, Figure 2C).
258 To assess non-specific effects of effectors on transcription, we performed global
259 transcriptome profiling of K562 cells stably transduced with these effectors by RNA-seq (Figure
260 2D,E). Consistent with the growth assay, cells expressing SID-dCas9-Kox1 had globally
261 perturbed transcription, with 4282 genes differentially expressed compared to control cells
262 expressing GFP only at $p<0.05$ (Figure 2E). Indeed, these samples clustered separately from
263 every other control and effector-expressing sample (Figure 2D). In addition, 53 genes were
264 differentially expressed in cells with dCas9-Kox1-MeCP2, suggesting that constitutive
265 expression of this effector also leads to minor non-specific effects on transcription (Figure 2E).
266 No more than 3 genes were detected to be differentially expressed in cells expressing any of the
267 other effectors, suggesting that these effectors do not non-specifically perturb transcription
268 (Figure 2E). Together, these results suggest that (over)expression of SID-dCas9-Kox1 is toxic
269 and globally perturbs transcription at least in K562 cells. We therefore excluded this effector
270 from further analysis.
271
272 *Zim3-dCas9 and dCas9-Kox1-MeCP2 mediate strongest knockdown*
273 We next sought to measure the efficacy of each effector in knocking down targeted genes with
274 two complementary approaches: (i) measurement of growth phenotypes resulting from
275 knockdown of essential genes, i.e. genes required for the growth or survival of dividing human
276 cells, and (ii) direct measurement of knockdown of cell surface proteins (Figure 3A, Table S8).
277 In both assays, we used single-sgRNA expression cassettes, which allowed us to use previously
278 validated strong and intermediate-activity sgRNAs (Jost et al., 2020). We included intermediate-

279 activity sgRNAs for two reasons: First, activity differences between effectors are more apparent
280 when knockdown is not saturated. Second, as it can be challenging to identify sgRNAs with high
281 activity across genes and cell types, effectors that mediate strong knockdown even with
282 imperfect sgRNAs could reduce false negative rates in genetic screens.

283 We measured growth phenotypes resulting from knockdown of essential genes using
284 internally normalized competitive growth assays. We transduced K562 cell lines stably
285 expressing each CRISPRi effector with vectors simultaneously expressing an sgRNA and a
286 fluorescent marker (mCherry) at a low multiplicity of infection (0.2-0.5). We then monitored the
287 ratio of sgRNA-expressing cells (mCherry+) and unperturbed cells (mCherry-) by flow
288 cytometry, with the expectation that cells with an essential gene-targeting sgRNA would deplete
289 at a rate proportional to CRISPRi activity. We targeted three genes, alanyl-tRNA synthetase
290 (*AARS*), the mitochondrial inner membrane import factor DNAJC19, and subunit D of RNA
291 polymerase I and III (*POLR1D*), with three different sgRNAs each. For all sgRNAs tested,
292 sgRNA-expressing cells depleted at the fastest rate with Zim3-dCas9 and at the second-fastest
293 rate with either dCas9-Kox1 or dCas9-Kox1-MeCP2 (Figures 3B, Figure S3A).

294 Next, to directly measure depletion of targeted proteins, we knocked down the non-
295 essential cell surface proteins CD55 (complement decay-accelerating factor), CD81 (TAPA-1/
296 TSPAN28), and CD151 (TSPAN24) and measured staining intensity with fluorescently labeled
297 antibodies by flow cytometry as a proxy for protein levels. We transduced K562 lines stably
298 expressing the different CRISPRi effectors with vectors expressing either targeting or non-
299 targeting sgRNAs at a low multiplicity of infection (0.2-1). Six days after transduction, we
300 stained cells with fluorescently labeled antibodies against the different cell surface proteins and
301 assessed knockdown by comparing the median antibody staining intensity in cells expressing a
302 targeting sgRNA and cells expressing a non-targeting control sgRNA. With strong sgRNAs,
303 Zim3-dCas9, dCas9-Kox1, and dCas9-Kox1-MeCP2 all mediated strong depletion of each cell
304 surface protein (>96.8% median depletion for all effectors and sgRNAs). With weak sgRNAs,
305 dCas9-Kox1-MeCP2 mediated the strongest knockdown closely followed by Zim3-dCas9,
306 whereas dCas9-Kox1 mediated weaker knockdown (Figures 3C, 3D, Figure S3B-D).

307 Importantly, flow cytometry reports on expression at the single-cell level, allowing us to
308 assess cell-to-cell heterogeneity in knockdown, which is missed when quantifying median
309 expression. As a proxy for heterogeneity, we calculated the fraction of cells without evidence of

310 knockdown despite the use of a strong sgRNA (Figure 3E). For Zim3-dCas9, knockdown was
311 largely homogeneous, with only ~5% of cells without detectable knockdown (Figures 3D, 3E,
312 Figure S3B-D), perhaps due to the presence of some senescent cells in the population in which
313 lack of cell division limits protein dilution. By contrast, for dCas9-Kox1-MeCP2, 15-20% of
314 cells did not achieve knockdown (Figures 3D, 3E, Figure S3B-D). This result may be explained
315 by the toxicity of the effector protein leading to selection against effector expression (Figure 2C)
316 or may be indicative of an intrinsic property of MeCP2 activity. The observed heterogeneity in
317 MeCP2 knockdown may help explain why dCas9-Kox1-MeCP2 appears to mediate the strongest
318 median knockdown while Zim3-dCas9 leads to faster dropout of sgRNA-expressing cells in the
319 essential gene growth assay; in the growth assay, heterogeneity would lead to worse performance
320 due to selection against strong knockdown. In sum, these results suggest that the Zim3-dCas9
321 effector confers strong knockdown that is homogeneous across a cell population.
322
323 *A versatile collection of Zim3-dCas9 constructs for robust knockdown across cell types*
324 To assess the general utility of the Zim3-dCas9 effector, we measured knockdown efficacy in
325 different cell types. For each cell type, we constructed cell lines stably expressing Zim3-dCas9
326 (see *Methods*; Supplementary Note 4) and measured knockdown of cell surface proteins by flow
327 cytometry. In both RPE1 (retinal pigment epithelium) and Jurkat (acute T-cell leukemia) cells,
328 cells expressing Zim3-dCas9 had stronger knockdown than previously reported cell lines
329 expressing dCas9-Kox1 (Figure 4A) (Horlbeck et al., 2018; Jost et al., 2017). Zim3-dCas9 also
330 conferred strong and homogeneous knockdown in HepG2 (hepatocellular carcinoma), HT29
331 (colorectal adenocarcinoma), and HuTu-80 (duodenal adenocarcinoma) cells (Figure 4B, Figure
332 S4).
333 To further maximize utility of the Zim3-dCas9 effector, we generated a panel of
334 constructs for expression of Zim3-dCas9 from the SFFV or EF1α promoters linked to BFP, GFP,
335 or mCherry (Table S7). We also generated backbones to express effectors from additional
336 promoters (CMV, EFS) and with different types of C-terminal fluorescent protein linkages (P2A,
337 IRES, direct fusion) (Table S7). In addition, as the bright fluorescence from the fluorescent
338 proteins may be undesirable in some settings, we generated a construct in which expression of
339 Zim3-dCas9 is linked to a hygromycin resistance marker [Zim3-dCas9 (Hygro)]. K562 cells
340 stably transduced with Zim3-dCas9 (Hygro) and selected with hygromycin for 4 weeks had

341 strong and homogeneous knockdown that was indistinguishable from knockdown in a cell line
342 generated by FACS (Figure 4C). Finally, we generated constructs in which the fluorescent
343 protein is flanked by LoxP sites, such that the fluorescent protein can be removed by transient
344 delivery of Cre once a stable cell line has been generated (Table S7). All of our constructs are
345 available via Addgene. Our collection of Zim3-dCas9 expression constructs and streamlined
346 protocols enables robust CRISPRi across a broad range of cell models.
347
348 **Discussion**
349 High-quality genetic screening approaches are catalysts for basic research and drug development.
350 Among the available approaches, CRISPRi has several appealing features including
351 independence of double-stranded DNA breaks, homogeneity and reversibility of perturbations,
352 accessibility of partial loss-of-function phenotypes, and compatibility with direct measurements
353 of target gene expression levels in both bulk populations and single cells. CRISPRi screens have
354 indeed propelled biological discovery in several contexts, but broader deployment has been
355 limited by difficulties in generating CRISPRi cell models and limited knockdown efficacy for a
356 subset of genes. Here, we present a suite of tools and accompanying protocols to address these
357 limitations and improve the efficacy and accessibility of CRISPRi.
358 Our ultra-compact, dual-sgRNA CRISPRi library confers stronger knockdown and
359 growth phenotypes than previously reported libraries and thus should minimize false-negative
360 rates in screens. Nonetheless, this library also has drawbacks. First, some library elements
361 undergo intermolecular recombination during lentiviral transduction. We can detect and
362 computationally remove such recombination events, such that they do not corrupt the resulting
363 data. As a consequence, recombination primarily decreases effective library coverage, and in
364 return cell numbers need to be increased by ~20-30% to ensure coverage. In the future,
365 recombination may be further mitigated using decoy vectors, different promoters, and
366 alternatively processed guides (Adamson et al., 2016; Dong et al., 2017; Feldman et al., 2018;
367 Knapp et al., 2019). Second and perhaps more importantly, screens will be inherently noisier and
368 sensitive to off-target effects with only a single element per gene, such that in standard cell lines
369 in which cell numbers are not a concern, existing single-sgRNA libraries may remain the
370 approach of choice. Inclusion of the 3-4 and 5-6 element sublibraries in our dual-sgRNA library
371 can mitigate this noise at the expense of some of the compactness. In cases in which cell

372 numbers are limited by the model, time, or cost, however, the compactness of our dual-sgRNA
373 library will be transformative. Examples include screens in primary or stem-cell derived models
374 or *in vivo* as well as screens with high-content readout such as Perturb-seq (Bock et al., 2022;
375 Przybyla and Gilbert, 2021). Additionally, this dual-sgRNA strategy may provide similar
376 benefits for other CRISPR modalities such as CRISPR-mediated overexpression (CRISPR
377 activation, CRISPRa), as also described by others (Yin et al., 2022), and we have designed a
378 dual-sgRNA CRISPRa library for this purpose (Table S9). Finally, the improved knockdown
379 afforded by the dual-sgRNA approach will also be beneficial in arrayed experiments, in which
380 recombination is not a concern, and we have included a protocol for cloning dual-sgRNA
381 libraries in array (Supplementary Note 3). In sum, our dual-sgRNA libraries improve CRISPRi
382 knockdown and complement existing libraries by broadening the scope of models in which
383 CRISPRi screens are feasible.

384 In the realm of CRISPRi effectors, our work points to a clear consensus: Zim3-dCas9 is
385 the effector of choice, as it appears equal or superior to other effectors in every test we
386 performed and had no downsides. We had previously measured by Perturb-seq that Zim3-dCas9
387 afforded median mRNA knockdown of 91.6% across 2,285 genes in RPE1 cells (Replogle et al.,
388 2022), and here we further found that Zim3-dCas9 mediates robust knockdown across a range of
389 cell types. Our work highlights the importance of using multiple assays to assess effector
390 function including single-cell assays to assess cell-to-cell heterogeneity, of directly measuring
391 knockdown instead of relying on proxies such as growth phenotypes that conflate multiple
392 factors, and of evaluating effectors in stably transduced cells rather than in transiently transfected
393 cells to evaluate longer-term consequences for cell viability. To facilitate implementation of
394 CRISPRi in additional cell models, we created a suite of effector expression constructs with
395 different combinations of promoters and markers (Table S7) as well as a cell line generation
396 protocol (Supplementary Note 4).

397 Nonetheless, there is more progress to be made in evaluating effectors and generating
398 robust CRISPRi models. First, our comparison of the effectors was not exhaustive. For example,
399 although we expressed all effectors from the same context, we did not control for potential
400 differences in expression levels or nuclear localization across effectors. The Zim3-dCas9
401 expression constructs appear optimal as they are, but activities of other effectors may be boosted
402 by optimizing these factors. Second, repression of gene expression is generally mediated through

403 recruitment of endogenous cofactors; for KRAB domains such as those from Zim3 and Kox1,
404 this endogenous cofactor is TRIM28 (Ecco et al., 2017). TRIM28 expression varies by cell type,
405 and efficacy of Zim3 and Kox1 may be limited in cell types with low TRIM28 expression. In
406 such cell types, the MeCP2 effector may be a suitable alternative, but the selection against
407 effector-expressing cells may increase false positive and false negative rates. Third, we did not
408 measure if the effectors differed in propensity for sgRNA-dependent off-target effects. Previous
409 work on dCas9-Kox1 had documented that well-designed sgRNAs have minimal off-target
410 effects (Gilbert et al., 2013). The main source of off-target effects of CRISPRi are at
411 bidirectional promoters, which likely is an inevitable consequence of the mechanism of
412 CRISPRi. We note that the stronger activity of Zim3-based effectors may amplify such effects.
413 For now, such off-target effects can be readily predicted and measured, for example by Perturb-
414 seq (Replogle et al., 2022). Perhaps future efforts will identify strategies to limit knockdown of
415 neighboring genes. Finally, in some cell types effector expression is silenced over time, leading
416 to loss of CRISPRi activity. We described some strategies to counteract such silencing
417 (Supplementary Note 4), but further protection against silencing remains as an area for
418 improvement. In any case, the assays we describe may be used to test additional effectors in a
419 streamlined and standardized fashion, with the goal of making CRISPRi universally available
420 across cell models.
421 Altogether, our resources and best practices will guide both current implementations and
422 future developments of CRISPRi. All our protocols, constructs, cell lines, and libraries are
423 available as resources to the community.
424

425 **Acknowledgements**
426 We thank B. Adamson, J. Nuñez, J. Hussmann, M. Horlbeck, E. Chow, S. Gupta, and F. Urnov
427 for helpful discussions. We thank M. de Vera, S. Sinha, C. Muresan, and J. Kanter for lab and
428 administrative support. We thank I. Aifantis (NYU) for donating a vector containing SID4x and
429 G. Ow and E. Collisson (UCSF) for donating the mCherry-marked sgRNA expression vector.
430 We thank the UCSF Center for Advanced Technology for sequencing, the Whitehead Institute
431 Flow Cytometry Core and the Harvard Immunology Flow Cytometry Core Facility for access to
432 FACS machines and flow cytometers, and the Whitehead Institute Genome Technology Core for
433 performing bulk RNA-seq library preparation.

Funding

This work was supported in part by the National Institutes of Health (grants R00GM130964 to MJ and RM1HG009490-01 to JSW), Springer Nature Global Grant for Gut Health 1772808 (MJ), a Charles H. Hood Foundation Child Health Research Award (MJ), DARPA HR0011-19-2-0007 (JSW), the Ludwig Center at MIT (JSW), and the Chan Zuckerberg Initiative (JSW). JMR was supported by NIH F31 Ruth L. Kirschstein National Research Service Award NS115380. KL was supported by NIH F30 Ruth L. Kirschstein National Research Service Award AG066418. BJR was supported by Harvard Bacteriology PhD Training Program T32 AI132120. AG was supported by Human Frontier Science Program grant 2019L/LT000858. MK was supported by the Chan Zuckerberg Initiative Ben Barres Early Career Acceleration Award. JSW is a Howard Hughes Medical Institute Investigator.

Competing Interests

JMR consults for Maze Therapeutics and Waypoint Bio. TMN consults for Maze Therapeutics. MK serves on the Scientific Advisory Boards of Engine Biosciences, Casma Therapeutics, Cajal Neuroscience, and Alector, and is an advisor to Modulo Bio and Recursion Therapeutics. MJ consults for Maze Therapeutics and Gate Bioscience. LAG declares outside interest in Chroma Medicine. JSW declares outside interest in 5 AM Venture, Amgen, Chroma Medicine, KSQ Therapeutics, Maze Therapeutics, Tenaya Therapeutics, Tessera Therapeutics, and Third Rock Ventures. The Regents of the University of California with TMN, MJ, LAG, and JSW as inventors have filed patent applications related to CRISPRi/a screening and Perturb-seq. LAG, MK, and JSW are inventors on US Patent 11,254,933 related to CRISPRi/a screening.

Author Contributions

JMR generated and tested dual-sgRNA libraries, created dual-sgRNA cloning and sequencing protocols, and analyzed screen and Perturb-seq data. JLB generated Zim3-dCas9 expression constructs, generated K562 cell lines, assayed effects on growth and transcription, and measured knockdown in K562 cells. ANP cloned dual-sgRNA libraries, performed screens and Perturb-seq, generated sequencing libraries, and generated and validated Jurkat and RPE1 cells expressing Zim3-dCas9. CRL generated effector expression constructs and performed

465 preliminary tests. NKM generated additional Zim3-dCas9 expression constructs. NKM, YD,
466 BJR, and XW generated and measured knockdown in HepG2, HuTu-80, and HT-29 cells
467 expressing Zim3-dCas9. AG generated Zim3-dCas9 (Hygro) and validated the corresponding
468 K562 cell line. TMN helped with effector testing. RAP generated IRES-linked effector
469 expression constructs. KL and MK provided screen data and helped with data aggregation.
470 DMR, MEW, and LAG provided unpublished screen data. JMR, JLB, and MJ wrote the
471 manuscript with guidance from JSW and input from all authors. MK, JSW, and MJ obtained
472 funding. JSW and MJ supervised all work.
473

474 **Materials Availability**

475 All sgRNA expression plasmids, sgRNA libraries, and effector expression plasmids are available
476 via Addgene, with accession numbers listed in Table S7. All new CRISPRi cell lines are
477 available from the corresponding authors.

478

479 **Data and Code Availability**

480 Python scripts for alignment of sequencing data from dual-sgRNA screens with and without
481 IBCs are available here: https://github.com/josephreplogle/CRISPRi-dual-sgRNA-screens.
482 Sequencing data are available on NCBI GEO under accession number GSE205310 (Perturb-seq)
483 and GSE205147 (bulk RNA-seq).

484

485 **Materials and Methods**

486 *Cell line generation and maintenance*

487 K562 cells were grown in RPMI 1640 medium with 25 mM HEPES, 2 mM L-glutamine, 2 g/L
488 $NaHCO_3$ (Gibco) supplemented with 10% (v/v) standard fetal bovine serum (FBS, VWR), 100
489 units/mL penicillin, 100 µg/mL streptomycin, and 2 mM L-glutamine (Gibco). hTERT-
490 immortalized RPE1 cells (ATCC CRL-4000) were grown in DMEM:F12 (Gibco) supplemented
491 with 10% (v/v) standard FBS (VWR), 0.01 mg/mL hygromycin B, 100 units/mL penicillin, and
492 100 µg/mL streptomycin. Jurkat cells (Clone E6-1, ATCC TIB-152) were grown in RPMI 1640
493 medium with 25 mM HEPES, 2 mM L-glutamine, 2 g/L $NaHCO_3$ (Gibco) supplemented with
494 10% (v/v) standard FBS (VWR), 100 units/mL penicillin, 100 µg/mL streptomycin, and 2 mM L-
495 glutamine (Gibco). HepG2 (ATCC HB-8065) and HuTu-80 cells (ATCC HTB-40) were grown
496 in Eagle's Minimum Essential Medium with 1.5 g/L NaHCO3, 110 mg/L sodium pyruvate, 292
497 mg/L L-glutamine (Corning) supplemented with 10% (v/v) standard FBS (R&D Systems), 100
498 units/mL penicillin, and 100 µg/mL streptomycin (Gibco). HT29 cells (ATCC HTB-38) were
499 grown in DMEM with 25 mM D-glucose, 3.7 g/L $NaHCO_3$, 4 mM L-glutamine (Gibco)
500 supplemented with 10% (v/v) standard FBS (R&D Systems), 100 units/mL penicillin, and 100
501 ug/mL streptomycin (Gibco). HEK293T cells were grown in Dulbecco's modified eagle medium
502 (DMEM) with 25 mM D-glucose, 3.7 g/L $NaHCO_3$, 4 mM L-glutamine (Gibco) and
503 supplemented with 10% (v/v) standard FBS (VWR or R&D Systems), 100 units/mL penicillin,
504 100 µg/mL streptomycin, and 2 mM L-glutamine (Gibco). K562 (chronic myelogenous

505 leukemia) and HT29 (colorectal adenocarcinoma) cells are derived from female patients. Jurkat
506 (acute T-cell leukemia), HuTu-80 (duodenal adenocarcinoma), and HepG2 (hepatocellular
507 carcinoma) cells are derived from male patients. HEK293T (embryonic kidney) cells are derived
508 from a female fetus. RPE1 (immortalized retinal pigment epithelium) cells are derived from a
509 female subject. All cell lines were grown at 37 °C in the presence of 5% CO_2.
510 To generate the K562 cell lines stably expressing various CRISPRi effectors, parental
511 K562 cells were stably transduced with lentiviral vectors expressing the corresponding effectors
512 linked to GFP via a P2A ribosome skipping sequence from an SFFV promoter with an upstream
513 ubiquitous chromatin opening element (UCOE). Polyclonal populations of GFP-positive cells
514 were selected using two rounds of fluorescence-activated cell sorting (FACS) on a Sony SH800S
515 Cell Sorter.
516 To generate RPE1 cells stably expressing Zim3-dCas9, RPE-1 cells were infected with
517 lentivirus containing UCOE-SFFV-Zim3-dCas9-P2A-BFP (pJB108) at low multiplicity of
518 infection by centrifugation at 1000 × g. Polyclonal populations of BFP-positive cells were
519 selected using two rounds of FACS on a Sony SH800S Cell Sorter. To generate Jurkat cells
520 stably expressing Zim3-dCas9, Jurkat cells were infected with virus containing UCOE-EF1α-
521 Zim3-dCas9-P2A-mCh (pJB109) at low multiplicity of infection by centrifugation at 1000 × g.
522 Polyclonal populations of mCherry-positive cells were selected using two rounds of FACS on a
523 Sony SH800S Cell Sorter. To generate HepG2, HuTu-80, and HT29 cells stably expressing
524 Zim3-dCas9, cells were infected with lentivirus containing UCOE-EF1α-Zim3-dCas9-P2A-mCh
525 (pJB109) at low multiplicity of infection. Polyclonal populations of mCherry-positive cells were
526 selected using two rounds of FACS on a FACSAria II Cell Sorter (BD Biosciences). To generate
527 K562 cells stably expressing Zim3-dCas9 without a fluorescent marker, K562 cells were infected
528 with virus containing UCOE-SFFV-Zim3-dCas9-P2A-hygro (pAG389) at low multiplicity of
529 infection by centrifugation at 1000 × g. To select for a polyclonal population, cells were treated
530 48 hours after infection with 200 µg/mL hygromycin for one week, followed by treatment 500
531 µg/ml hygromycin for three weeks.
532
533 *Lentivirus production*
534 Lentivirus was generated by transfecting HEK239T cells with the transfer plasmid and four
535 packaging plasmids (for expression of VSV-G, Gag/Pol, Rev, and Tat) using TransIT-LT1

536 Transfection Reagent (Mirus Bio). Viral supernatant was harvested two days after transfection
537 and filtered through 0.44 µm PES filters and/or frozen at –80 °C prior to transduction.
538
539 *Design and cloning of pilot genome-wide single- and dual-sgRNA CRISPRi libraries*
540 To compare the use of single- and dual-sgRNA CRISPRi libraries in systematic genetic screens,
541 pilot genome-wide single- and dual-sgRNA CRISPRi libraries were designed and cloned.
542 sgRNAs targeting each gene were selected from our previously published hCRISPRi v2 library
543 by balancing empirical data from previous genetic screens with Horlbeck *et al.* predicted
544 rankings (Horlbeck et al., 2016a) using a three-tiered approach:
545 Tier 1. For genes essential for growth in the K562 CRISPRi screen data (p-value < 0.001
546 and $\gamma < -0.2$) (Horlbeck et al., 2016a), sgRNAs were ranked by their growth phenotype.
547 Tier 2. As many genetic perturbations only cause a conditional cellular phenotype (e.g.,
548 in a particular cell type, chemical stressor, or reporter phenotype), we next aggregated data
549 across multiple genetic screens (only a subset of the data in Table S3 was available for the pilot
550 library design). For genes that were identified as a significant hit [FDR 0.05 based on MAGeCK
551 RRA p-value (Li et al., 2014)] in previous CRISPRi screens, sgRNAs were ranked by the sum of
552 z-scored phenotypes across screens.
553 Tier 3. For all other genes, sgRNAs were ranked by the regression scores in hCRISPRi
554 v2.1 (Horlbeck et al., 2016a).
555 Using this ranking scheme, we selected the single best sgRNA for a single-
556 sgRNA/single-element-per-gene library (dJR004) and the two best sgRNAs for a dual-
557 sgRNA/single-element-per-gene library (dJR020). A list of sgRNA targeting sequences both the
558 single and dual sgRNA libraries is available in Table S1.
559 The single-sgRNA library dJR004 was cloned using the protocol described here:
560 https://weissman.wi.mit.edu/resources/Pooled_CRISPR_Library_Cloning.pdf. A modified
561 CROP-seq sgRNA lentiviral expression vector (pJR107) was derived from the parental vector
562 pBA950 (https://www.addgene.org/122239/) by incorporating a GFP fluorescent marker and a
563 UCOE element upstream of the EF1alpha promoter to prevent marker silencing. sgRNA
564 targeting sequences were appended with flanking sequence, BstX1/BlpI overhangs, and PCR
565 adapters. The library was synthesized as an oligonucleotide pool (Twist Biosciences), PCR-
566 amplified, BstX1/BlpI-digested, and inserted into pJR107 by ligation.

567 The dual-sgRNA library dJR020 was cloned using the protocol in Supplementary Note 1.
568 Briefly, dual-sgRNA targeting sequences were spaced by a BsmBI-cut site and appended with
569 flanking sequence, BstX1/BlpI overhangs, and PCR adapters with the structure: with the
570 structure: 5'- PCR adaptor - CCACCTTGTTG – targeting sequence A -
571 gtttcagagcgagacgtgcctgcaggatacgtctcagaaacatg – targeting sequence B -
572 GTTTAAGAGCTAAGCTG - PCR adaptor-3'. The library was synthesized as an
573 oligonucleotide pool (Twist Biosciences), PCR-amplified, BstX1/BlpI-digested, and inserted into
574 pJR104 by ligation. Next, the sgRNA CR3/hU6 promoter insert pJR98 was BsmBI-digested and
575 ligated into the BsmBI-digested library to generate the final library. In the final library, each
576 element expresses two unique sgRNAs from tandem U6 expression cassettes.
577
578 *Genome-wide growth screens for library comparison*
579 Parallel growth screens were performed to compare dJR004 versus dJR020. Lentivirus from
580 dJR004 and dJR020 was produced in HEK293T as described above. CRISPRi K562 cells
581 expressing dCas9-KOX1 KRAB were spinfected (1000G) with polybrene (8 ug/ml) with lentivirus
582 from dJR004 and dJR020 in biological replicate. Throughout the screen, cells were maintained at
583 a density between 250,000 – 1,000,000 cells per ml and 1000X coverage per library element. On
584 day 3 post-transduction, an infection rate of 11%-18% was measured by GFP fluorescence. On
585 day 3 through day 6 post-transduction, puromycin at 1 ug/ml was used to select for infected cells,
586 and cells were allowed to recover for two days. On day 8 post-transduction, a cell pellet was frozen
587 for each replicate representing the initial sample (T_0) of the screen. Throughout the screen, the
588 number of cell doublings was recorded, and final samples (T_{final}) were collected on day 20 post-
589 transduction.
590
591 *Screen library preparation, sequencing, and analysis*
592 Amplicon DNA libraries were prepared from cell pellets as previously described (Nuñez et al.,
593 2021). Genomic DNA was isolated using a NucleoSpin Blood XL kit or NucleoSpin Blood L kit
594 (Macherey–Nagel) depending on pellet size. Purified genomic DNA was directly amplified by
595 22 cycles of PCR using NEBNext Ultra II Q5 PCR MasterMix (NEB). Sequencing was
596 performed on a NovaSeq 6000 (Illumina) using a 19 bp Read 1, 19 bp Read 2, and 5 bp Index
597 Read 1 with custom sequencing primers.

598 After sequencing, sgRNA sequencing reads were aligned to the single and dual sgRNA
599 libraries using a custom Python script without allowing mismatches. Reads for which the Read 1
600 and Read 2 sgRNA sequences did not target the same gene likely arose from lentiviral
601 recombination and were discarded from downstream analysis. For both replicates of the dual-
602 sgRNA library, 29.4%, of mapped reads contained sgRNAs targeting different genes. Library
603 elements (*i.e.*, sgRNAs or sgRNA pairs) represented with 0 sequencing reads were assigned a
604 pseudocount of 1 read, while library elements represented with fewer than 50 sequencing reads
605 in both T_0 and T_{final} of any screen replicate were excluded from analysis. For each sgRNA or
606 sgRNA pair, the growth phenotype (γ) was defined as the $\log_2$(sgRNA normalized count T_{final} /
607 sgRNA normalized T_0) – median non-targeting control $\log_2$(sgRNA normalized count T_{final} /
608 sgRNA normalized count T_0), divided by the replicate total cell doublings and normalized to the
609 total number of sequencing reads for a given sample (Gilbert et al., 2014). Read counts and
610 growth phenotypes of library elements are included in Table S2. For the analysis of the Cancer
611 Dependency Map (DepMap) Common Essential genes, the 20Q1 Common Essential genes were
612 downloaded from https://depmap.org/portal/download/. For receiver operating characteristic
613 (ROC) curve analysis, "positives" were defined as genes with a K562 CRISPRi growth screen *p*-
614 value < 0.001 and γ < -0.05 (Horlbeck et al., 2016a), and "negatives" were defined as non-
615 targeting control guide pairs.
616
617 *Empirical sgRNA selection, incorporation of integration barcodes, and validation of finalized*
618 *dual-sgRNA CRISPRi libraries*
619 While the pilot dual-sgRNA library dJR020 enabled validation of the dual-sgRNA strategy,
620 finalized dual-sgRNA libraries were designed with additional considerations. An expanded set of
621 aggregated CRISPR screen data was used to optimize guide selection, including data from
622 screens previously published in (Adamson et al., 2016; Brown et al., 2022; Das et al., 2021; Hein
623 and Weissman, 2022; Hickey et al., 2020; Horlbeck et al., 2016; Jost et al., 2020, 2017; Lou et
624 al., 2019; Martinko et al., 2018; Ramkumar et al., 2020; Shao et al., 2022, 2018; Tian et al.,
625 2021, 2019; Torres et al., 2019; Vasseur et al., 2021) (Table S3). Optimal sgRNAs targeting each
626 gene were selected using an updated set of rules. First, sgRNAs containing a BsmBI target
627 sequence (CGTCTC or GAGACG) were removed to avoid dropout during cloning. Second, each
628 transcript per gene in Horlbeck *et al.*, 2016a was targeted independently. Genes were separated

629 into three tiers, similar to the tiers described for the pilot library but with additional
630 considerations:
631 Tier 1 (n=662 genes). For genes essential for growth in the K562 CRISPRi screen data
632 (p-value < 0.001 and $\gamma < -0.2$) (Horlbeck et al., 2016a), sgRNAs were ranked by their growth
633 phenotypes (calculated relative to the best-performing sgRNA targeting each gene per screen in
634 which the gene was a significant hit at FDR 0.05).
635 Tier 2 (n=4,033 genes): The ranking strategy used to generate the pilot library (dJR020)
636 included any gene identified as a significant hit in any previous CRISPRi screen for empirical
637 guide selection and as such did not control for the increased chance that a gene may score as a
638 false positive in a screen as the number of screens increases (the equivalent of multiple
639 comparisons). To control for such false positives, the 320 olfactory genes served as a negative
640 control set. None of the 320 olfactory genes were a significant hit [FDR 0.05 based on MAGeCK
641 RRA p-value (Li et al., 2014)] in greater than four previous CRISPRi screens. Therefore, as a
642 first cutoff, any gene that was identified as a significant hit in five or more previous CRISPRi
643 screens, regardless of the strength of the phenotype, was included in this tier.
644 This cutoff misses genes that score strongly, and as such are high-confidence hits, in a
645 small number of screens. To also include such genes, each gene that was a significant hit [FDR
646 0.05 based on MAGeCK RRA p-value (Li et al., 2014)] in one to four screens was assigned a
647 score based on the maximum absolute value discriminant score (calculated as the $-\log_{10} p$-value
648 multiplied by the mean z-scored phenotype of the top three sgRNAs), summed across screens in
649 which the gene scored as a hit. As a comparison, this same score was calculated for olfactory
650 genes. Genes were included in this tier if the discriminant score was greater than a threshold
651 calculated from the olfactory gene scores for the same number of screens in which a gene was
652 identified as a hit.
653 For all genes included in this tier, sgRNAs were ranked by the average of phenotypes
654 across screens in which the gene was identified as a hit. Only sgRNAs that were identified as a
655 hit at FDR<0.01 in at least one screen were ranked. sgRNA phenotypes were calculated relative
656 to the best performing sgRNA targeting each gene per screen in which the gene was a significant
657 hit at FDR 0.05.
658 Tier 3 (n=14,493 genes): For all other genes, sgRNAs were ranked by the regression
659 scores in hCRISPRi v2.1 (Horlbeck et al., 2016a).

660 Using this ranking scheme, we selected the first and second ranked sgRNAs for a dual-
661 sgRNA/single-element-per-gene sublibrary (hCRISPRi_dual_1_2), the third and fourth ranked
662 sgRNAs for a second dual-sgRNA/single-element-per-gene sublibrary (hCRISPRi_dual_3_4),
663 and the fifth and sixth ranked sgRNAs for a final dual-sgRNA/single-element-per-gene
664 sublibrary (hCRISPRi_dual_5_6). Each library also contains a set of non-targeting control dual
665 sgRNAs representing 5% of the total library elements. A list of sgRNA targeting sequences for
666 all libraries is available in Table S4.
667 Integration barcodes (IBCs) were incorporated between the tandem sgRNA cassettes in
668 the dual-sgRNA library in four steps. First, a library of 215 8-nucleotide IBCs were designed
669 with a Hamming distance ≥ 4 and between 25-75% GC content (Table S5). Second, the library of
670 IBCs were cloned into pJR98 in an arrayed format. pJR98 was digested by AscI and ssDNA
671 oligo donors of the sequence 5' CTCTTCCTGCCCGACCTTGGGG – reverse complement IBC
672 – CAGCGCCATAGCTGAGTGTAGATTCGAGC – 3' were cloned into the vector using
673 NEBuilder HiFI DNA Assembly Master Mix (NEB). Third, the library of cloned IBCs were
674 Sanger verified and pooled at a equimolar ratio for all barcodes. Fourth, the library was cloned
675 into the dual-sgRNA library by BsmBI-digestion and ligation. Sequencing was performed on a
676 NovaSeq 6000 (Illumina) using a 19 bp Read 1, 19 bp Read 2, 8 bp Index Read 1, and 8 bp Index
677 Read 2 with custom sequencing primers as described in Supplementary Note 2. Demultiplexing
678 on only the i5 index using the i7 index (IBC) as a read was performed as detailed:
679 https://gist.github.com/sumeetg23/a064a36801d2763e94da2e191699fb9f.
680
681 *Perturb-seq comparison of dual sgRNA libraries versus Dolcetto*
682 Direct capture Perturb-seq (Replogle et al., 2020) was used to directly compare the knockdown
683 produced by the dual-sgRNA libraries versus the Dolcetto Set A CRISPRi library. N=128 genes
684 were randomly selected from the 4,000 most highly-expressed genes in K562 cells based on
685 RNA-seq (https://www.encodeproject.org/experiments/ENCSR000AEL/). Two parallel libraries
686 were cloned: a library containing the three dual-sgRNA elements targeting each gene and a
687 library containing the three Dolcetto Set A guides targeting each gene, plus non-targeting control
688 guides. For Dolcetto sgRNAs, the 5′ base was replaced with a G to enable expression from the
689 U6 promoter. The Dolcetto single-sgRNA library was cloned as described above into pJR101
690 guide expression vector containing a Perturb-seq capture sequence in stem loop 2. The dual-

691 sgRNA library cloned as described above into pJR101 with a pJR98 insert cassette containing a
692 Perturb-seq capture sequence in stem loop 2 of guide B. After library verification by sequencing,
693 lentivirus was prepared in HEK293T as described above.
694 For Perturb-seq, CRISPRi K562 cells expressing dCas9-KOX1 KRAB (Gilbert et al.,
695 2014) were spinfected (1000 × *g*) with polybrene (8 µg/ml) with lentivirus from both libraries in
696 parallel. Throughout the screen, cells were maintained at a density between 250,000 – 1,000,000
697 cells per ml and 1000× coverage per library element. On day 3 post-transduction, an infection rate
698 of 5% was measured for both screens, and infected cells were sorted by FACS (BD FACS Aria).
699 On day 7 post-transduction, cells were prepared for single-cell RNA-sequencing as detailed in the
700 10x Genomics Single Cell Protocols Cell Preparation Guide (10x Genomics, CG00053 Rev C)
701 and separated into droplet emulsions using the Chromium Controller (10x Genomics) with
702 Chromium Single-Cell 3′ Gel Beads v3.1 (10x Genomics, PN-1000121 and PN-1000120) across
703 12 lanes/gemgroups with the goal of recovering ~15,000 cells per GEM group before filtering.
704 Sequencing libraries were prepared following the 10x Genomics Chromium Single Cell 3' Reagent
705 Kits User Guide (v3.1 Chemistry) with Feature Barcoding technology for CRISPR Screening
706 (CG000205; Rev C). Libraries were sequenced on a NovaSeq 6000 (Illumina) according to the
707 10x Genomics User Guide.
708 After sequencing, mRNA and sgRNA counts were obtained from Cell Ranger 4.0.0
709 software (10x Genomics). To assign guides to cells, we used a Poisson-Gaussian mixture model
710 as previously described (Replogle et al., 2020). Only cells bearing a single Dolcetto sgRNA or a
711 single dual-sgRNA guide B sgRNA were used for downstream calculation of CRISPRi efficacy.
712 For each guide, the on-target knockdown was calculated as the fraction of mRNA remaining (target
713 gene expression in targeting cells relative to cells bearing non-targeting control guides).
714
715 *Design and cloning of constructs for CRISPRi effector expression*
716 All CRISPRi effectors were cloned into a lentiviral backbone containing a ubiquitous chromatin
717 opening element and a spleen focus forming virus (SFFV) promoter (pMH0001, Addgene #
718 85969). Briefly, dCas9, effector domains, linker domains, and GFP were PCR amplified and
719 inserted into backbone linearized by digest with MluI and NotI using Gibson assembly
720 (NEBuilder HiFI DNA Assembly Master Mix, NEB). P2A sequences were incorporated into

721 primer overhangs. The following additional considerations were incorporated into the final
722 construct designs:

723 1) For KRAB from Kox1, the KRAB(KOX1) domain from dCas9-BFP-KRAB (Addgene #
724 46911) was fused to the C-terminus of dCas9, because C-terminal fusions of
725 KRAB(KOX1) have historically produced the highest activity, linked by an 80-amino
726 acid linker (XTEN80). XTEN80-KRAB(KOX1) was synthesized as a gBlock (IDT). We
727 chose XTEN80 because we previously found that inclusion of a linker increases activity
728 and the original dCas9-BFP-KRAB(KOX1) construct (Gilbert et al., 2013) underwent
729 proteolytic cleavage between dCas9 and KRAB(KOX1) in some cell types, giving rise to
730 free dCas9, a dominant negative for CRISPRi. The final construct is dCas9-XTEN80-
731 KRAB(KOX1) or dCas9-Kox1 for short.

732 2) KRAB(ZIM3) was fused to the N-terminus of dCas9 with a 6-amino acid GS linker,
733 which had produced the highest activity in a previous report, including when compared to
734 C-terminal fusions (Alerasool et al., 2020). KRAB(ZIM3) was PCR-amplified from
735 pLX303-ZIM3-KRAB-dCas9 (Addgene # 154472). The final construct is KRAB(ZIM3)-
736 dCas9 or Zim3-dCas9 for short. Note that this construct contains an additional nuclear
737 localization signal between Zim3 and dCas9.

738 3) For SID4x, SID4x was fused to the N-terminus of dCas9-XTEN80-KRAB(Kox1),
739 because SID4x had previously only been evaluated for CRISPRi in the context of a dual
740 fusion (Carleton et al., 2017). A shorter 16-aa linker (XTEN16) was included between
741 SID4x and dCas9, which has been a sufficient linker length at the N-terminus in the past.
742 SID4x was amplified from a construct generously donated by the Aifantis lab (New York
743 University). The final construct is SID4x-XTEN16-dCas9-XTEN80-KRAB(KOX1) or
744 SID-dCas9-Kox1 for short.

745 4) For MeCP2, the previously reported dCas9-KRAB(Kox1)-MeCP2 construct (Addgene #
746 110821; Yeo et al., 2018) was PCR-amplified and transferred into the common backbone,
747 giving rise to dCas9-Kox1-MeCP2. Note that this construct contains no linker between
748 dCas9 and KRAB(Kox1), such that the KRAB(Kox1) domain may be largely inactive,
749 and that the dCas9 uses different codons. We separately also generated a construct in
750 which we fused MeCP2 to the C-terminus of the dCas9-XTEN80-KRAB(KOX1)

751 construct. We observed similar growth defects and non-specific effects on the
752 transcriptome using this construct.
753 Additional constructs with expression driven by a EF1α promoter were generated by performing
754 analogous assemblies in the pMH0006 backbone (Addgene # 135448). Constructs with
755 expression driven by CMV or EFS promoters were generated by replacing the SFFV promoter in
756 existing constructs. Constructs in which effector expression is marked with BFP, mCherry, or
757 hygromycin resistance were generated by assembling with PCR products containing the desired
758 markers. Constructs in which expression of the fluorescent protein is linked by an internal
759 ribosome entry site (IRES) from encephalomyocarditis virus (EMCV) were generated by
760 incorporating a PCR fragment generated from pHR-TRE3G-TUBB-IRES-mCherry (Jost et al.,
761 2017) instead of the P2A site. Constructs in which EGFP is flanked by loxP sites were generated
762 by PCR-amplifying EGFP with primers containing loxP 2272 sequences
763 (ATAACTTCGTATAAaGTATcCTATACGAAGTTAT). The amplicon was inserted by Gibson
764 Assembly into pJB069 or pJB109 linearized by digestion with NotI and AsiSI. Finally,
765 constructs in which the fluorescent proteins are constitutively linked to dCas9 were generated by
766 omitting the P2A sequence from primer overhangs. A full list of generated constructs is included
767 in Table S7. All constructs are available on Addgene.
768
769 *Evaluation of effects of CRISPRi effectors on growth and transcription*
770 K562 cell lines stably expressing CRISPRi effectors from an SFFV promoter linked to GFP via
771 P2A were generated by lentiviral transduction and FACS. Each effector expression construct was
772 transduced in triplicate in parallel with all other constructs. 100,000 GFP-positive cells per
773 replicate were isolated by FACS on a Sony SH800S Cell Sorter 5 d after transduction and
774 allowed to recover.
775 To generate RNA-seq libraries of cells expressing each effector, 1×10^6 cells were
776 harvested for each sample 6 d after FACS by centrifugation at 300 × *g* for 5 min and flash frozen
777 in a dry ice and ethanol bath. RNA was extracted using the Direct-zol RNA Miniprep kit (Zymo
778 Research) and quantified using the Qubit RNA BR Assay Kit (Life Technologies). RNA-seq
779 libraries were prepared by the Whitehead Genome Technology Core facility using the Roche
780 Diagnostics KAPA mRNA HyperPrep Kit. Paired-end 100 sequencing was performed on a
781 NovaSeq (Illumina).

782 To evaluate growth of CRISPRi effector-expressing cells, a reference population of K562
783 cells stably expressing mCherry was generated by lentiviral transduction of pU6-sgRNA
784 EF1Alpha-puro-T2A-mCherry (a gift from Gregory Ow and Eric Collisson, UCSF) and FACS.
785 This was conducted in parallel with the generation of CRISPRi effector-expressing cells. 7 days
786 after sorting, ~125,000 cells per GFP-sorted population (different CRISPRi effectors) were
787 mixed with ~125,000 mCherry-sorted cells (reference population). The ratio of mCherry-positive
788 to mCherry-negative cells was read out immediately after mixing and periodically for the next 19
789 days by flow cytometry on an Attune NxT (ThermoFisher).
790
791 *RNA-seq data analysis*
792 Sequencing reads were aligned strand-specifically to the human genome (GRCh38) and then
793 aggregated by gene using only reads uniquely mapped to the reverse strand using the spliced
794 read aligner STAR (Dobin et al., 2013), version 2.7.9, against an index containing features from
795 Ensembl release 98 / GENCODE v32 (downloaded from 10x Genomics reference 2020-A).
796 Replicate sample 2 for cells expressing dCas9-Kox1 had substantially fewer reads than expected
797 and was excluded from analysis. For clustering analysis, transcript counts were normalized to
798 transcripts per million for each sample, filtered for the 2000 most highly expressed genes on
799 average, and clustered using the Ward variance minimization algorithm implemented in scipy
800 version 1.6.2. Differential expression analysis was carried out on gene counts using DESeq2
801 (Love et al., 2014). For Figure 2E, transcript counts were not filtered. The trends for numbers of
802 differentially expressed genes were equivalent when only including genes with an average count
803 > 2 across all samples.
804
805 *Selection and cloning of individual sgRNAs*
806 Strong sgRNAs against essential genes or cell surface markers were selected from the
807 hCRISPRi-v2 library (Horlbeck et al., 2016a; Nuñez et al., 2021). Intermediate-activity sgRNAs
808 were selected either from the hCRISPRi-v2 library or by incorporating defined mismatches in
809 strong sgRNAs (Jost et al., 2020). All sgRNA sequences used for individual evaluation are listed
810 in Table S7.
811 Individual sgRNA expression constructs were cloned as described previously (Gilbert et
812 al., 2014). Briefly, two complementary oligonucleotides (IDT), containing the sgRNA targeting

813 region as well as overhangs matching those left by restriction digest of the vector with BstXI and
814 BlpI, were annealed and ligated into pCRISPRia-v2 [pU6-sgRNA EF1Alpha-puro-T2A-BFP
815 with two SbfI sites flanking the sgRNA expression cassette, Addgene #84832 (Horlbeck et al.,
816 2016a)] or pU6-sgRNA EF1Alpha-puro-T2A-mCherry [a gift from Gregory Ow and Eric
817 Collisson, UCSF, (Jost et al., 2020)] digested with BstXI (NEB or Thermo Fisher Scientific) and
818 BlpI (NEB) or Bpu1102I (Thermo Fisher Scientific). The ligation product was transformed into
819 Stellar chemically competent *E. coli* cells (Takara Bio) and plasmid was prepared following
820 standard protocols. The resulting sgRNA expression vectors were individually packaged into
821 lentivirus as described above.
822
823 *Evaluation of individual sgRNA phenotypes*
824 Effects of sgRNAs targeting essential genes on cell growth were measured in internally
825 controlled growth assays by transducing cells with mCherry-marked sgRNA expression
826 constructs at MOI < 0.5 (15 – 40% infected cells) and measuring the fraction of sgRNA-
827 expressing cells 3-12 days after transduction as mCherry-positive cells by flow cytometry on an
828 Attune NxT (ThermoFisher). All experiments were performed in duplicates from the infection
829 step.
830 Effects of sgRNAs on expression levels of cell surface proteins were measured by flow
831 cytometry. K562 or Jurkat cell lines expressing CRISPRi effectors of interest were infected with
832 lentivirus containing sgRNA expression vectors by centrifugation at 1000 × *g* for 1 h in 24-well
833 plates in the presence of 8 µg/mL polybrene (Sigma-Aldrich). RPE1, HepG2, HuTu-80, and
834 HT29 cell lines expressing Zim3-dCas9 were infected with lentivirus containing sgRNA
835 expression vectors for 24 h in the presence of 8 µg/mL polybrene. 6-14 d after transduction, cells
836 were harvested by centrifugation (suspension cells) or trypsin-free detachment (adherent cells;
837 mechanical detachment or EDTA), washed once in flow cytometry buffer (PBS with 5% (v/v)
838 FBS), and stained at room temperature for 15-30 min with APC-conjugated antibodies targeting
839 CD55 (clone JS11, BioLegend 311311, RRID AB_2075857), CD81 (clone 5A6, Biolegend
840 349509, RRID AB_2564020), CD151 (clone 50-6, BioLegend 350405, RRID AB_10661726),
841 CD29 (clone TS2/16, Biolegend 303007, RRID AB_314323), or B2M (clone 2M2, Biolegend
842 316312, RRID AB_10641281) diluted 1:100 in flow cytometry buffer. After staining, cells were
843 washed twice in 200 µL flow cytometry buffer and resuspended in flow cytometry buffer for

844 measurement on an Attune NxT (ThermoFisher), LSR-II (BD Biosciences) or Symphony A3
845 (BD Biosciences).
846 Optimal dilutions for each antibody were determined by testing 1:20, 1:100, and 1:500
847 antibody titrations on K562 cells with epitope-targeting or non-targeting sgRNAs and choosing
848 the titration with the maximum signal difference.
849 Flow cytometry data were analyzed using FlowCytometryTools 0.5.0
850 (https://eyurtsev.github.io/FlowCytometryTools/) and python 3.8. Briefly, the data were gated
851 for cells (FSC-A versus SSC-A), FSC singlets (FSC-W versus FSC-H for data recorded on an
852 Attune NxT and FSC-W versus FSC-A for data recorded on an LSR-II), SSC singlets (SSC-W
853 versus SSC-H for data recorded on an Attune NxT and SSC-W versus SSC-A for data recorded
854 on an LSR-II), and sgRNA-expressing cells (BFP- or mCherry-positive, depending on the
855 experiment). Background APC fluorescence intensity from unstained cells or cells stained with
856 an APC-conjugated Mouse IgG1, κ isotype control (BioLegend clone MOPC-21) was subtracted
857 to correct for background fluorescence. Knockdown was quantified using median background-
858 corrected APC fluorescence intensity in cells expressing a targeting sgRNA relative to intensity
859 in cells expressing a non-targeting control sgRNA, with the exception of the Jurkat and RPE1
860 experiments, for which knockdown was quantified using median background-corrected APC
861 fluorescence intensity in cells expressing a targeting sgRNA relative to intensity in cells not
862 expressing an sgRNA in the same well.
863

References

Adamson B, Norman TM, Jost M, Cho MY, Nuñez JK, Chen Y, Villalta JE, Gilbert LA, Horlbeck MA, Hein MY, Pak RA, Gray AN, Gross CA, Dixit A, Parnas O, Regev A, Weissman JS. 2016. A Multiplexed Single-Cell CRISPR Screening Platform Enables Systematic Dissection of the Unfolded Protein Response. *Cell* 167:1867-1882.e21. doi:10.1016/j.cell.2016.11.048

Adamson B, Norman TM, Jost M, Weissman JS. 2018. Approaches to maximize sgRNA-barcode coupling in Perturb-seq screens. *Biorxiv* 298349. doi:10.1101/298349

Alerasool N, Segal D, Lee H, Taipale M. 2020. An efficient KRAB domain for CRISPRi applications in human cells. *Nat Methods* 17:1093–1096. doi:10.1038/s41592-020-0966-x

Behan FM, Iorio F, Picco G, Gonçalves E, Beaver CM, Migliardi G, Santos R, Rao Y, Sassi F, Pinnelli M, Ansari R, Harper S, Jackson DA, McRae R, Pooley R, Wilkinson P, Meer D van der, Dow D, Buser-Doepner C, Bertotti A, Trusolino L, Stronach EA, Saez-Rodriguez J, Yusa K, Garnett MJ. 2019. Prioritization of cancer therapeutic targets using CRISPR–Cas9 screens. *Nature* 568:511–516. doi:10.1038/s41586-019-1103-9

Bock C, Datlinger P, Chardon F, Coelho MA, Dong MB, Lawson KA, Lu T, Maroc L, Norman TM, Song B, Stanley G, Chen S, Garnett M, Li W, Moffat J, Qi LS, Shapiro RS, Shendure J, Weissman JS, Zhuang X. 2022. High-content CRISPR screening. *Nat Rev Methods Primers* 2:8. doi:10.1038/s43586-021-00093-4

Bosch B, DeJesus MA, Poulton NC, Zhang W, Engelhart CA, Zaveri A, Lavalette S, Ruecker N, Trujillo C, Wallach JB, Li S, Ehrt S, Chait BT, Schnappinger D, Rock JM. 2021. Genome-wide gene expression tuning reveals diverse vulnerabilities of M. tuberculosis. *Cell* 184:4579-4592.e24. doi:10.1016/j.cell.2021.06.033

Bowden AR, Morales-Juarez DA, Sczaniecka-Clift M, Agudo MM, Lukashchuk N, Thomas JC, Jackson SP. 2020. Parallel CRISPR-Cas9 screens clarify impacts of p53 on screen performance. *Elife* 9:e55325. doi:10.7554/elife.55325

Brown A-L, Wilkins OG, Keuss MJ, Hill SE, Zanovello M, Lee WC, Bampton A, Lee FCY, Masino L, Qi YA, Bryce-Smith S, Gatt A, Hallegger M, Fagegaltier D, Phatnani H, Phatnani H, Kwan J, Sareen D, Broach JR, Simmons Z, Arcila-Londono X, Lee EB, Deerlin VMV, Shneider NA, Fraenkel E, Ostrow LW, Baas F, Zaitlen N, Berry JD, Malaspina A, Fratta P, Cox GA, Thompson LM, Finkbeiner S, Dardiotis E, Miller TM, Chandran S, Pal S, Hornstein E, MacGowan DJ, Heiman-Patterson T, Hammell MG, Patsopoulos NikolaosA, Butovsky O, Dubnau J, Nath A, Bowser R, Harms M, Aronica E, Poss M, Phillips-Cremins J, Crary J, Atassi N, Lange DJ, Adams DJ, Stefanis L, Gotkine M, Baloh RH, Babu S, Raj T, Paganoni S, Shalem O, Smith C, Zhang B, Harris B, Broce I, Drory V, Ravits J, McMillan C, Menon V, Wu L, Altschuler S, Lerner Y, Sattler R, Keuren-Jensen KV, Rozenblatt-Rosen O, Lindblad-Toh K, Nicholson K, Gregersen P, Lee J-H, Kokos S, Muljo S, Newcombe J, Gustavsson EK, Seddighi S, Reyes JF, Coon SL, Ramos D, Schiavo G, Fisher EMC, Raj T, Secrier M, Lashley T, Ule J, Buratti E, Humphrey J, Ward ME, Fratta P. 2022. TDP-43 loss and ALS-risk SNPs drive mis-splicing and depletion of UNC13A. *Nature* 603:131–137. doi:10.1038/s41586-022-04436-3

Carleton JB, Berrett KC, Gertz J. 2017. Multiplex Enhancer Interference Reveals Collaborative Control of Gene Regulation by Estrogen Receptor α-Bound Enhancers. *Cell Syst* 5:333-344.e5. doi:10.1016/j.cels.2017.08.011

910 Coukos R, Yao D, Sanchez MI, Strand ET, Olive ME, Udeshi ND, Weissman JS, Carr SA,
911 Bassik MC, Ting AY. 2021. An engineered transcriptional reporter of protein localization
912 identifies regulators of mitochondrial and ER membrane protein trafficking in high-
913 throughput CRISPRi screens. *Elife* 10:e69142. doi:10.7554/elife.69142
914 Das R, Sjöström M, Shrestha R, Yogodzinski C, Egusa EA, Chesner LN, Chen WS, Chou J,
915 Dang DK, Swinderman JT, Ge A, Hua JT, Kabir S, Quigley DA, Small EJ, Ashworth A, Feng
916 FY, Gilbert LA. 2021. An integrated functional and clinical genomics approach reveals genes
917 driving aggressive metastatic prostate cancer. *Nat Commun* 12:4601. doi:10.1038/s41467-
918 021-24919-7
919 Dobin A, Davis CA, Schlesinger F, Drenkow J, Zaleski C, Jha S, Batut P, Chaisson M, Gingeras
920 TR. 2013. STAR: ultrafast universal RNA-seq aligner. *Bioinformatics* 29:15–21.
921 doi:10.1093/bioinformatics/bts635
922 Doench JG. 2018. Am I ready for CRISPR? A user's guide to genetic screens. *Nat Rev Genet*
923 19:67–80. doi:10.1038/nrg.2017.97
924 Dong F, Xie K, Chen Y, Yang Y, Mao Y. 2017. Polycistronic tRNA and CRISPR guide-RNA
925 enables highly efficient multiplexed genome engineering in human cells. *Biochem Bioph Res*
926 *Co* 482:889–895. doi:10.1016/j.bbrc.2016.11.129
927 Dräger NM, Sattler SM, Huang CT-L, Teter OM, Leng K, Hashemi SH, Hong J, Aviles G,
928 Clelland CD, Zhan L, Udeochu JC, Kodama L, Singleton AB, Nalls MA, Ichida J, Ward ME,
929 Faghri F, Gan L, Kampmann M. 2022. A CRISPRi/a platform in iPSC-derived microglia
930 uncovers regulators of disease states. Biorxiv 2021.06.16.448639.
931 doi:10.1101/2021.06.16.448639
932 Du D, Roguev A, Gordon DE, Chen M, Chen S-H, Shales M, Shen JP, Ideker T, Mali P, Qi LS,
933 Krogan NJ. 2017. Genetic interaction mapping in mammalian cells using CRISPR
934 interference. *Nat Methods* 14:577–580. doi:10.1038/nmeth.4286
935 Ecco G, Imbeault M, Trono D. 2017. KRAB zinc finger proteins. *Development* 144:2719–2729.
936 doi:10.1242/dev.132605
937 Feldman D, Singh A, Garrity AJ, Blainey PC. 2018. Lentiviral co-packaging mitigates the effects
938 of intermolecular recombination and multiple integrations in pooled genetic screens. *Biorxiv*
939 262121. doi:10.1101/262121
940 Fulco CP, Munschauer M, Anyoha R, Munson G, Grossman SR, Perez EM, Kane M, Cleary B,
941 Lander ES, Engreitz JM. 2016. Systematic mapping of functional enhancer–promoter
942 connections with CRISPR interference. *Science* 354:769–773. doi:10.1126/science.aag2445
943 Fulco CP, Nasser J, Jones TR, Munson G, Bergman DT, Subramanian V, Grossman SR, Anyoha
944 R, Doughty BR, Patwardhan TA, Nguyen TH, Kane M, Perez EM, Durand NC, Lareau CA,
945 Stamenova EK, Aiden EL, Lander ES, Engreitz JM. 2019. Activity-by-Contact model of
946 enhancer-promoter regulation from thousands of CRISPR perturbations. *Nat Genet* 51:1664–
947 1669. doi:10.1038/s41588-019-0538-0
948 Gasperini M, Hill AJ, McFaline-Figueroa JL, Martin B, Kim S, Zhang MD, Jackson D, Leith A,
949 Schreiber J, Noble WS, Trapnell C, Ahituv N, Shendure J. 2019. A Genome-wide Framework
950 for Mapping Gene Regulation via Cellular Genetic Screens. *Cell* 176:377-390.e19.
951 doi:10.1016/j.cell.2018.11.029
952 Gilbert LA, Horlbeck MA, Adamson B, Villalta JE, Chen Y, Whitehead EH, Guimaraes C,
953 Panning B, Ploegh HL, Bassik MC, Qi LS, Kampmann M, Weissman JS. 2014. Genome-
954 Scale CRISPR-Mediated Control of Gene Repression and Activation. *Cell* 159:647–661.
955 doi:10.1016/j.cell.2014.09.029

956 Gilbert LA, Larson MH, Morsut L, Liu Z, Brar GA, Torres SE, Stern-Ginossar N, Brandman O,
957 Whitehead EH, Doudna JA, Lim WA, Weissman JS, Qi LS. 2013. CRISPR-Mediated
958 Modular RNA-Guided Regulation of Transcription in Eukaryotes. *Cell* 154:442–451.
959 doi:10.1016/j.cell.2013.06.044
960 Haapaniemi E, Botla S, Persson J, Schmierer B, Taipale J. 2018. CRISPR–Cas9 genome editing
961 induces a p53-mediated DNA damage response. *Nat Med* 24:927–930. doi:10.1038/s41591-
962 018-0049-z
963 Haswell JR, Mattioli K, Gerhardinger C, Maass PG, Foster DJ, Peinado P, Wang X, Medina PP,
964 Rinn JL, Slack FJ. 2021. Genome-wide CRISPR interference screen identifies long non-
965 coding RNA loci required for differentiation and pluripotency. *Plos One* 16:e0252848.
966 doi:10.1371/journal.pone.0252848
967 Hawkins JS, Silvis MR, Koo B-M, Peters JM, Osadnik H, Jost M, Hearne CC, Weissman JS,
968 Todor H, Gross CA. 2020. Mismatch-CRISPRi Reveals the Co-varying Expression-Fitness
969 Relationships of Essential Genes in Escherichia coli and Bacillus subtilis. *Cell Syst* 11:523-
970 535.e9. doi:10.1016/j.cels.2020.09.009
971 Hein MY, Weissman JS. 2022. Functional single-cell genomics of human cytomegalovirus
972 infection. *Nat Biotechnol* 40:391–401. doi:10.1038/s41587-021-01059-3
973 Hickey KL, Dickson K, Cogan JZ, Replogle JM, Schoof M, D'Orazio KN, Sinha NK, Hussmann
974 JA, Jost M, Frost A, Green R, Weissman JS, Kostova KK. 2020. GIGYF2 and 4EHP Inhibit
975 Translation Initiation of Defective Messenger RNAs to Assist Ribosome-Associated Quality
976 Control. *Mol Cell* 79:950-962.e6. doi:10.1016/j.molcel.2020.07.007
977 Hill AJ, McFaline-Figueroa JL, Starita LM, Gasperini MJ, Matreyek KA, Packer J, Jackson D,
978 Shendure J, Trapnell C. 2018. On the design of CRISPR-based single-cell molecular screens.
979 *Nat Methods* 15:271–274. doi:10.1038/nmeth.4604
980 Horlbeck MA, Gilbert LA, Villalta JE, Adamson B, Pak RA, Chen Y, Fields AP, Park CY, Corn
981 JE, Kampmann M, Weissman JS. 2016a. Compact and highly active next-generation libraries
982 for CRISPR-mediated gene repression and activation. *Elife* 5:e19760. doi:10.7554/elife.19760
983 Horlbeck MA, Witkowsky LB, Guglielmi B, Replogle JM, Gilbert LA, Villalta JE, Torigoe SE,
984 Tjian R, Weissman JS. 2016b. Nucleosomes impede Cas9 access to DNA in vivo and in vitro.
985 *Elife* 5:e12677. doi:10.7554/elife.12677
986 Horlbeck MA, Xu A, Wang M, Bennett NK, Park CY, Bogdanoff D, Adamson B, Chow ED,
987 Kampmann M, Peterson TR, Nakamura K, Fischbach MA, Weissman JS, Gilbert LA. 2018.
988 Mapping the Genetic Landscape of Human Cells. *Cell* 174:953-967.e22.
989 doi:10.1016/j.cell.2018.06.010
990 Ihry RJ, Worringer KA, Salick MR, Frias E, Ho D, Theriault K, Kommineni S, Chen J, Sondey
991 M, Ye C, Randhawa R, Kulkarni T, Yang Z, McAllister G, Russ C, Reece-Hoyes J, Forrester
992 W, Hoffman GR, Dolmetsch R, Kaykas A. 2018. p53 inhibits CRISPR–Cas9 engineering in
993 human pluripotent stem cells. *Nat Med* 24:939–946. doi:10.1038/s41591-018-0050-6
994 Jost M, Chen Y, Gilbert LA, Horlbeck MA, Krenning L, Menchon G, Rai A, Cho MY, Stern JJ,
995 Prota AE, Kampmann M, Akhmanova A, Steinmetz MO, Tanenbaum ME, Weissman JS.
996 2017. Combined CRISPRi/a-Based Chemical Genetic Screens Reveal that Rigosertib Is a
997 Microtubule-Destabilizing Agent. *Mol Cell* 68:210-223.e6. doi:10.1016/j.molcel.2017.09.012
998 Jost M, Santos DA, Saunders RA, Horlbeck MA, Hawkins JS, Scaria SM, Norman TM,
999 Hussmann JA, Liem CR, Gross CA, Weissman JS. 2020. Titrating gene expression using
1000 libraries of systematically attenuated CRISPR guide RNAs. *Nat Biotechnol* 38:355–364.
1001 doi:10.1038/s41587-019-0387-5

1002 Kearns NA, Pham H, Tabak B, Genga RM, Silverstein NJ, Garber M, Maehr R. 2015. Functional
1003 annotation of native enhancers with a Cas9 -histone demethylase fusion. *Nat Methods*
1004 12:401–403. doi:10.1038/nmeth.3325
1005 Klann TS, Black JB, Chellappan M, Safi A, Song L, Hilton IB, Crawford GE, Reddy TE,
1006 Gersbach CA. 2017. CRISPR–Cas9 epigenome editing enables high-throughput screening for
1007 functional regulatory elements in the human genome. *Nat Biotechnol* 35:561–568.
1008 doi:10.1038/nbt.3853
1009 Knapp DJHF, Michaels YS, Jamilly M, Ferry QRV, Barbosa H, Milne TA, Fulga TA. 2019.
1010 Decoupling tRNA promoter and processing activities enables specific Pol-II Cas9 guide RNA
1011 expression. *Nat Commun* 10:1490. doi:10.1038/s41467-019-09148-3
1012 Kosicki M, Tomberg K, Bradley A. 2018. Repair of double-strand breaks induced by CRISPR–
1013 Cas9 leads to large deletions and complex rearrangements. *Nat Biotechnol* 36:765–771.
1014 doi:10.1038/nbt.4192
1015 Leng K, Rose IVL, Kim H, Xia W, Romero-Fernandez W, Rooney B, Koontz M, Li E, Ao Y,
1016 Wang S, Krawczyk M, TCW J, Goate A, Zhang Y, Ullian EM, Sofroniew MV, Fancy SPJ,
1017 Schrag MS, Lippmann ES, Kampmann M. 2022. CRISPRi screens in human astrocytes
1018 elucidate regulators of distinct inflammatory reactive states. Biorxiv 2021.08.23.457400.
1019 doi:10.1101/2021.08.23.457400
1020 Li W, Xu H, Xiao T, Cong L, Love MI, Zhang F, Irizarry RA, Liu JS, Brown M, Liu XS. 2014.
1021 MAGeCK enables robust identification of essential genes from genome-scale CRISPR/Cas9
1022 knockout screens. *Genome Biol* 15:554. doi:10.1186/s13059-014-0554-4
1023 Liang JR, Lingeman E, Luong T, Ahmed S, Muhar M, Nguyen T, Olzmann JA, Corn JE. 2020.
1024 A Genome-wide ER-phagy Screen Highlights Key Roles of Mitochondrial Metabolism and
1025 ER-Resident UFMylation. *Cell* 180:1160-1177.e20. doi:10.1016/j.cell.2020.02.017
1026 Liu SJ, Horlbeck MA, Cho SW, Birk HS, Malatesta M, He D, Attenello FJ, Villalta JE, Cho MY,
1027 Chen Y, Mandegar MA, Olvera MP, Gilbert LA, Conklin BR, Chang HY, Weissman JS, Lim
1028 DA. 2017. CRISPRi-based genome-scale identification of functional long noncoding RNA
1029 loci in human cells. *Science* 355. doi:10.1126/science.aah7111
1030 Lou K, Steri V, Ge AY, Hwang YC, Yogodzinski CH, Shkedi AR, Choi ALM, Mitchell DC,
1031 Swaney DL, Hann B, Gordan JD, Shokat KM, Gilbert LA. 2019. KRASG12C inhibition
1032 produces a driver-limited state revealing collateral dependencies. *Sci Signal* 12.
1033 doi:10.1126/scisignal.aaw9450
1034 Love MI, Huber W, Anders S. 2014. Moderated estimation of fold change and dispersion for
1035 RNA-seq data with DESeq2. *Genome Biol* 15:550. doi:10.1186/s13059-014-0550-8
1036 Luteijn RD, Zaver SA, Gowen BG, Wyman S, Garelis N, Onia L, McWhirter SM, Katibah GE,
1037 Corn JE, Woodward JJ, Raulet DH. 2019. SLC19A1 transports immunoreactive cyclic
1038 dinucleotides. *Nature* 573:434–438. doi:10.1038/s41586-019-1553-0
1039 Mandegar MA, Huebsch N, Frolov EB, Shin E, Truong A, Olvera MP, Chan AH, Miyaoka Y,
1040 Holmes K, Spencer CI, Judge LM, Gordon DE, Eskildsen TV, Villalta JE, Horlbeck MA,
1041 Gilbert LA, Krogan NJ, Sheikh SP, Weissman JS, Qi LS, So P-L, Conklin BR. 2016.
1042 CRISPR Interference Efficiently Induces Specific and Reversible Gene Silencing in Human
1043 iPSCs. *Cell Stem Cell* 18:541–553. doi:10.1016/j.stem.2016.01.022
1044 Martinko AJ, Truillet C, Julien O, Diaz JE, Horlbeck MA, Whiteley G, Blonder J, Weissman JS,
1045 Bandyopadhyay S, Evans MJ, Wells JA. 2018. Targeting RAS-driven human cancer cells
1046 with antibodies to upregulated and essential cell-surface proteins. *Elife* 7:e31098.
1047 doi:10.7554/elife.31098

1048 Meyers RM, Bryan JG, McFarland JM, Weir BA, Sizemore AE, Xu H, Dharia NV, Montgomery
1049 PG, Cowley GS, Pantel S, Goodale A, Lee Y, Ali LD, Jiang G, Lubonja R, Harrington WF,
1050 Strickland M, Wu T, Hawes DC, Zhivich VA, Wyatt MR, Kalani Z, Chang JJ, Okamoto M,
1051 Stegmaier K, Golub TR, Boehm JS, Vazquez F, Root DE, Hahn WC, Tsherniak A. 2017.
1052 Computational correction of copy number effect improves specificity of CRISPR–Cas9
1053 essentiality screens in cancer cells. *Nat Genet* 49:1779–1784. doi:10.1038/ng.3984
1054 Michlits G, Hubmann M, Wu S-H, Vainorius G, Budusan E, Zhuk S, Burkard TR, Novatchkova
1055 M, Aichinger M, Lu Y, Reece-Hoyes J, Nitsch R, Schramek D, Hoepfner D, Elling U. 2017.
1056 CRISPR-UMI: single-cell lineage tracing of pooled CRISPR–Cas9 screens. *Nat Methods*
1057 14:1191–1197. doi:10.1038/nmeth.4466
1058 Morgens DW, Chan C, Kane AJ, Weir NR, Li A, Dubreuil MM, Tsui CK, Hess GT, Lavertu A,
1059 Han K, Polyakov N, Zhou J, Handy EL, Alabi P, Dombroski A, Yao D, Altman RB, Sello JK,
1060 Denic V, Bassik MC. 2019. Retro-2 protects cells from ricin toxicity by inhibiting ASNA1-
1061 mediated ER targeting and insertion of tail-anchored proteins. *Elife* 8:e48434.
1062 doi:10.7554/elife.48434
1063 Nuñez JK, Chen J, Pommier GC, Cogan JZ, Replogle JM, Adriaens C, Ramadoss GN, Shi Q,
1064 Hung KL, Samelson AJ, Pogson AN, Kim JYS, Chung A, Leonetti MD, Chang HY,
1065 Kampmann M, Bernstein BE, Hovestadt V, Gilbert LA, Weissman JS. 2021. Genome-wide
1066 programmable transcriptional memory by CRISPR-based epigenome editing. *Cell* 184:2503-
1067 2519.e17. doi:10.1016/j.cell.2021.03.025
1068 Przybyla L, Gilbert LA. 2021. A new era in functional genomics screens. *Nat Rev Genet* 1–15.
1069 doi:10.1038/s41576-021-00409-w
1070 Raffeiner P, Hart JR, García-Caballero D, Bar-Peled L, Weinberg MS, Vogt PK. 2020. An
1071 MXD1-derived repressor peptide identifies noncoding mediators of MYC-driven cell
1072 proliferation. *Proc National Acad Sci* 117:6571–6579. doi:10.1073/pnas.1921786117
1073 Ramkumar P, Abarientos AB, Tian R, Seyler M, Leong JT, Chen M, Choudhry P, Hechler T,
1074 Shah N, Wong SW, Martin TG, Wolf JL, Roybal KT, Pahl A, Taunton J, Wiita AP,
1075 Kampmann M. 2020. CRISPR-based screens uncover determinants of immunotherapy
1076 response in multiple myeloma. *Blood Adv* 4:2899–2911.
1077 doi:10.1182/bloodadvances.2019001346
1078 Replogle JM, Norman TM, Xu A, Hussmann JA, Chen J, Cogan JZ, Meer EJ, Terry JM, Riordan
1079 DP, Srinivas N, Fiddes IT, Arthur JG, Alvarado LJ, Pfeiffer KA, Mikkelsen TS, Weissman
1080 JS, Adamson B. 2020. Combinatorial single-cell CRISPR screens by direct guide RNA
1081 capture and targeted sequencing. *Nat Biotechnol* 38:954–961. doi:10.1038/s41587-020-0470-
1082 y
1083 Replogle JM, Saunders RA, Pogson AN, Hussmann JA, Lenail A, Guna A, Mascibroda L,
1084 Wagner EJ, Adelman K, Lithwick-Yanai G, Iremadze N, Oberstrass F, Lipson D, Bonnar JL,
1085 Jost M, Norman TM, Weissman JS. 2022. Mapping information-rich genotype-phenotype
1086 landscapes with genome-scale Perturb-seq. *Cell*. doi:10.1016/j.cell.2022.05.013
1087 Sage C le, Lawo S, Panicker P, Scales TME, Rahman SA, Little AS, McCarthy NJ, Moore JD,
1088 Cross BCS. 2017. Dual direction CRISPR transcriptional regulation screening uncovers gene
1089 networks driving drug resistance. *Sci Rep-uk* 7:17693. doi:10.1038/s41598-017-18172-6
1090 Sanson KR, Hanna RE, Hegde M, Donovan KF, Strand C, Sullender ME, Vaimberg EW,
1091 Goodale A, Root DE, Piccioni F, Doench JG. 2018. Optimized libraries for CRISPR-Cas9
1092 genetic screens with multiple modalities. *Nat Commun* 9:5416. doi:10.1038/s41467-018-
1093 07901-8

1094 Schellenberger V, Wang C, Geething NC, Spink BJ, Campbell A, To W, Scholle MD, Yin Y,
1095 Yao Y, Bogin O, Cleland JL, Silverman J, Stemmer WPC. 2009. A recombinant polypeptide
1096 extends the in vivo half-life of peptides and proteins in a tunable manner. *Nat Biotechnol*
1097 27:1186–1190. doi:10.1038/nbt.1588
1098 Schmidt R, Steinhart Z, Layeghi M, Freimer JW, Bueno R, Nguyen VQ, Blaeschke F, Ye CJ,
1099 Marson A. 2022. CRISPR activation and interference screens decode stimulation responses in
1100 primary human T cells. *Sci New York N Y* 375:eabj4008. doi:10.1126/science.abj4008
1101 Semesta KM, Tian R, Kampmann M, Zastrow M von, Tsvetanova NG. 2020. A high-throughput
1102 CRISPR interference screen for dissecting functional regulators of GPCR/cAMP signaling.
1103 *Plos Genet* 16:e1009103. doi:10.1371/journal.pgen.1009103
1104 Shao H, Li X, Moses MA, Gilbert LA, Kalyanaraman C, Young ZT, Chernova M, Journey SN,
1105 Weissman JS, Hann B, Jacobson MP, Neckers L, Gestwicki JE. 2018. Exploration of
1106 Benzothiazole Rhodacyanines as Allosteric Inhibitors of Protein–Protein Interactions with
1107 Heat Shock Protein 70 (Hsp70). *J Med Chem* 61:6163–6177.
1108 doi:10.1021/acs.jmedchem.8b00583
1109 Shao H, Taguwa S, Gilbert L, Shkedi A, Sannino S, Guerriero CJ, Gale-Day ZJ, Young ZT,
1110 Brodsky JL, Weissman J, Gestwicki JE, Frydman J. 2022. A campaign targeting a conserved
1111 Hsp70 binding site uncovers how subcellular localization is linked to distinct biological
1112 activities. *Cell Chem Biol*. doi:10.1016/j.chembiol.2022.06.006
1113 Smits AH, Ziebell F, Joberty G, Zinn N, Mueller WF, Clauder-Münster S, Eberhard D, Savitski
1114 MF, Grandi P, Jakob P, Michon A-M, Sun H, Tessmer K, Bürckstümmer T, Bantscheff M,
1115 Steinmetz LM, Drewes G, Huber W. 2019. Biological plasticity rescues target activity in
1116 CRISPR knock outs. *Nat Methods* 16:1087–1093. doi:10.1038/s41592-019-0614-5
1117 Thakore PI, D'Ippolito AM, Song L, Safi A, Shivakumar NK, Kabadi AM, Reddy TE, Crawford
1118 GE, Gersbach CA. 2015. Highly specific epigenome editing by CRISPR-Cas9 repressors for
1119 silencing of distal regulatory elements. *Nat Methods* 12:1143–1149. doi:10.1038/nmeth.3630
1120 Tian R, Abarientos A, Hong J, Hashemi SH, Yan R, Dräger N, Leng K, Nalls MA, Singleton
1121 AB, Xu K, Faghri F, Kampmann M. 2021. Genome-wide CRISPRi/a screens in human
1122 neurons link lysosomal failure to ferroptosis. *Nat Neurosci* 24:1020–1034.
1123 doi:10.1038/s41593-021-00862-0
1124 Tian R, Gachechiladze MA, Ludwig CH, Laurie MT, Hong JY, Nathaniel D, Prabhu AV,
1125 Fernandopulle MS, Patel R, Abshari M, Ward ME, Kampmann M. 2019. CRISPR
1126 Interference-Based Platform for Multimodal Genetic Screens in Human iPSC-Derived
1127 Neurons. *Neuron* 104:239-255.e12. doi:10.1016/j.neuron.2019.07.014
1128 Torres SE, Gallagher CM, Plate L, Gupta M, Liem CR, Guo X, Tian R, Stroud RM, Kampmann
1129 M, Weissman JS, Walter P. 2019. Ceapins block the unfolded protein response sensor ATF6α
1130 by inducing a neomorphic inter-organelle tether. *Elife* 8:e46595. doi:10.7554/elife.46595
1131 Tsherniak A, Vazquez F, Montgomery PG, Weir BA, Kryukov G, Cowley GS, Gill S,
1132 Harrington WF, Pantel S, Krill-Burger JM, Meyers RM, Ali L, Goodale A, Lee Y, Jiang G,
1133 Hsiao J, Gerath WFJ, Howell S, Merkel E, Ghandi M, Garraway LA, Root DE, Golub TR,
1134 Boehm JS, Hahn WC. 2017. Defining a Cancer Dependency Map. *Cell* 170:564-576.e16.
1135 doi:10.1016/j.cell.2017.06.010
1136 Vasseur ML, Friedman J, Jost M, Xu J, Yamada J, Kampmann M, Horlbeck MA, Salemi MR,
1137 Phinney BS, Weissman JS, Nunnari J. 2021. Genome-wide CRISPRi screening identifies
1138 OCIAD1 as a prohibitin client and regulatory determinant of mitochondrial Complex III
1139 assembly in human cells. *Elife* 10:e67624. doi:10.7554/elife.67624

1140 Xie S, Cooley A, Armendariz D, Zhou P, Hon GC. 2018. Frequent sgRNA-barcode
1141 recombination in single-cell perturbation assays. *Plos One* 13:e0198635.
1142 doi:10.1371/journal.pone.0198635
1143 Yeo NC, Chavez A, Lance-Byrne A, Chan Y, Menn D, Milanova D, Kuo C-C, Guo X, Sharma
1144 S, Tung A, Cecchi RJ, Tuttle M, Pradhan S, Lim ET, Davidsohn N, Ebrahimkhani MR,
1145 Collins JJ, Lewis NE, Kiani S, Church GM. 2018. An enhanced CRISPR repressor for
1146 targeted mammalian gene regulation. *Nat Methods* 15:611–616. doi:10.1038/s41592-018-
1147 0048-5
1148 Yin JA, Frick L, Scheidmann MC, Trevisan C, Dhingra A, Spinelli A, Wu Y, Yao L, Vena DL,
1149 De Cecco E, Ging K, Liu T, Täger J, Rodriguez S, Guo J, Berry S, Losa M, Hornemann S,
1150 Kampmann M, Pelkmans L, Hoepfner D, Heutink P, Aguzzi A. 2022. Robust and Versatile
1151 Arrayed Libraries for Human Genome-Wide CRISPR Activation, Deletion and Silencing.
1152 *bioRxiv*. doi:10.1101/2022.05.25.493370
1153 Zhu S, Cao Z, Liu Z, He Y, Wang Y, Yuan P, Li W, Tian F, Bao Y, Wei W. 2019. Guide RNAs
1154 with embedded barcodes boost CRISPR-pooled screens. *Genome Biol* 20:20.
1155 doi:10.1186/s13059-019-1628-0
1156
1157
1158
1159

Figures and Figure Legends

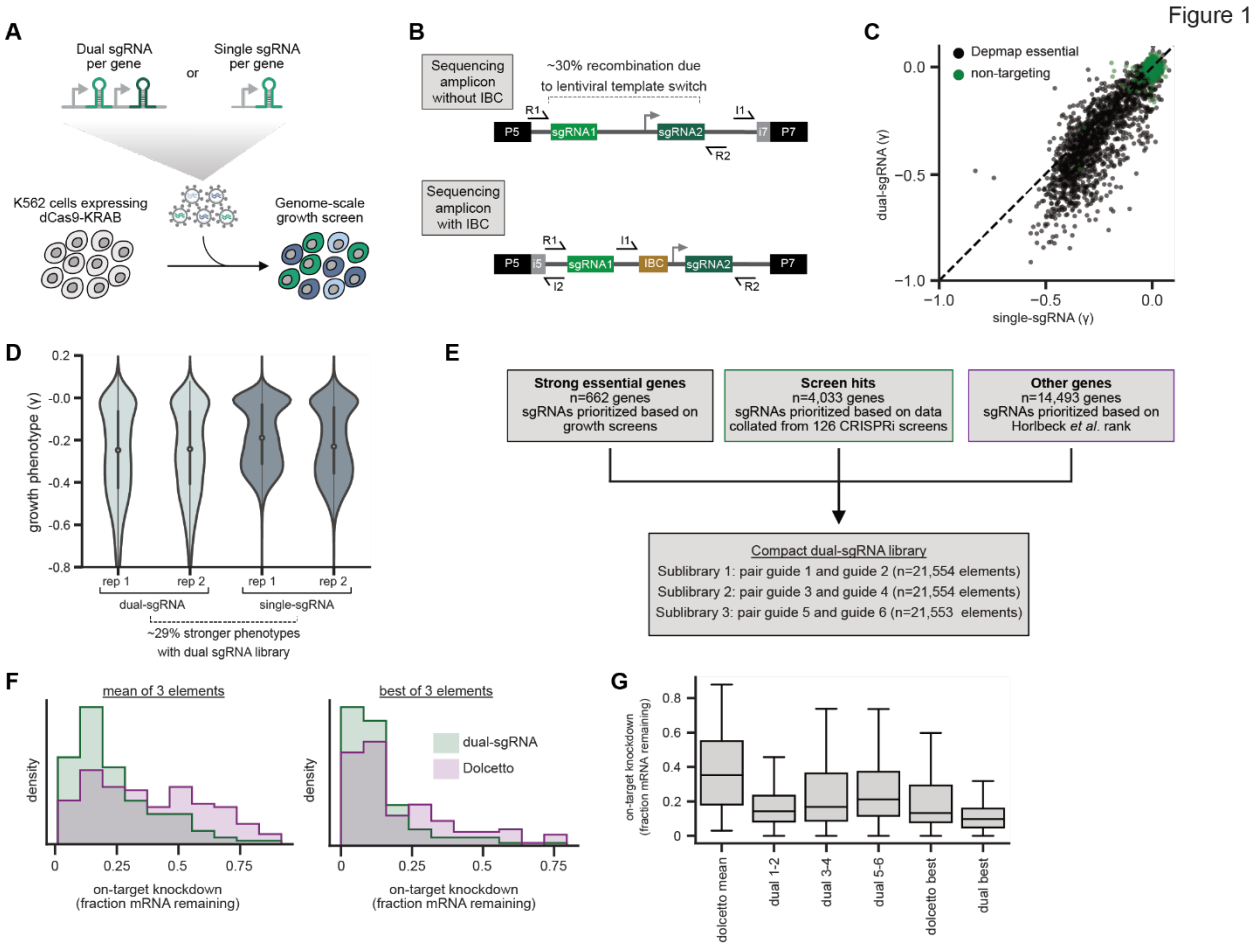

Figure 1. Design and validation of ultra-compact dual-sgRNA CRISPRi libraries.

a. Schematic of growth screen used to compare single- and dual-sgRNA libraries.

b. Schematic of dual-sgRNA library sequencing strategies.

c. Comparison of growth phenotypes for DepMap essential genes between single- and dual-sgRNA libraries. Sequencing libraries were prepared using the strategy labeled "Sequencing amplicon without IBC" in panel b. Growth phenotypes are reported as γ ($\log_2$ fold-enrichment of T_{final} over T_0, per doubling) and well-correlated between libraries ($r = 0.91$). Only values between -1 and 0.1 are shown.

d. Comparison of growth phenotypes for DepMap essential genes between single- and dual-sgRNA libraries. In the violin plot, the violin displays the kernel density estimate, the central white point represents the median, and the central black bar represents the interquartile range (IQR).

e. Design of final dual-sgRNA library.

1175 f. Comparison of target gene knockdown by dual-sgRNA library versus Dolcetto. Target gene
1176 knockdown was measured by single-cell RNA-sequencing (Perturb-seq). For each library, the
1177 "mean of 3 elements" was calculated as the mean knockdown of all three elements targeting each
1178 gene. The "best of 3 elements" represents the element with the best knockdown per each gene.
1179 g. Comparison of target gene knockdown across elements in dual-sgRNA library versus
1180 Dolcetto. In the box plot, the box shows the IQR, the line dividing the box shows the median
1181 value, and the whiskers extend to show 1.5x the IQR. Outlier observations >1.5x IQR are not
1182 shown.
1183
1184 See also Figure S1.
1185

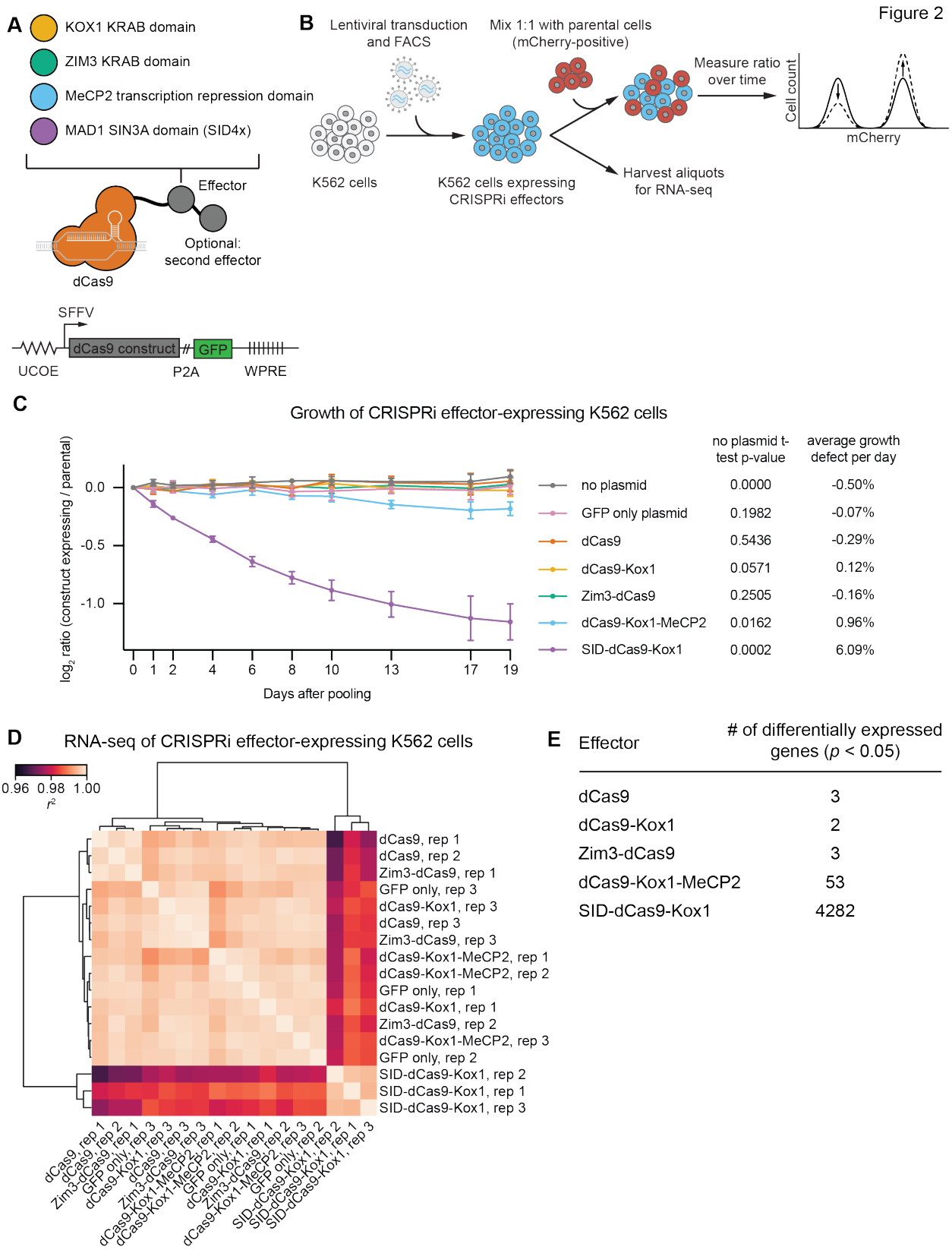

Figure 2. CRISPRi effectors containing SID or MeCP2 domains have non-specific effects

1188 **on cell viability and gene expression.**

1189 a. Schematics of CRISPRi transcription repressor domains and general lentiviral expression
1190 construct used for all CRISPRi effectors.

1191 b. Experimental design to test effects of stable expression of each CRISPRi effector on growth
1192 and transcription in K562 cells.

1193 c. Growth defects of effector-expressing cells, measured as the $\log_2$ ratio of mCherry-negative
1194 (effector-expressing) to mCherry-positive (not effector-expressing) cells in each well. mCherry
1195 levels were measured for 19 days after pooling cells. Data represent mean ± SD from three
1196 independent transductions of expression constructs. *p*-values are from an unpaired two-tailed t-
1197 test comparing D19 values for each sample to the D19 value for the ”no plasmid” sample.
1198 Average percent growth defect per day is the $\log_2$ D19 value divided by the number of days,
1199 multiplied by 100 for a percent value.

1200 d. Clustered heatmap of correlation of transcript counts from K562 cells expressing indicated
1201 CRISPRi effectors or a GFP control. Correlations across samples were calculated using
1202 normalized counts (reads per million) for all genes with mean normalized count >1 and then
1203 clustered using the Ward variance minimization algorithm implemented in scipy. r^2 is squared
1204 Pearson correlation. Data represent three independent transductions of expression constructs.

1205 e. Number of differentially expressed genes ($p < 0.05$) for cells expressing each effector versus
1206 cells expressing GFP only. *p*-values were calculated using a Wald test and corrected for multiple
1207 hypothesis testing as implemented in DeSeq2.

1208

1209 See also Figure S2.

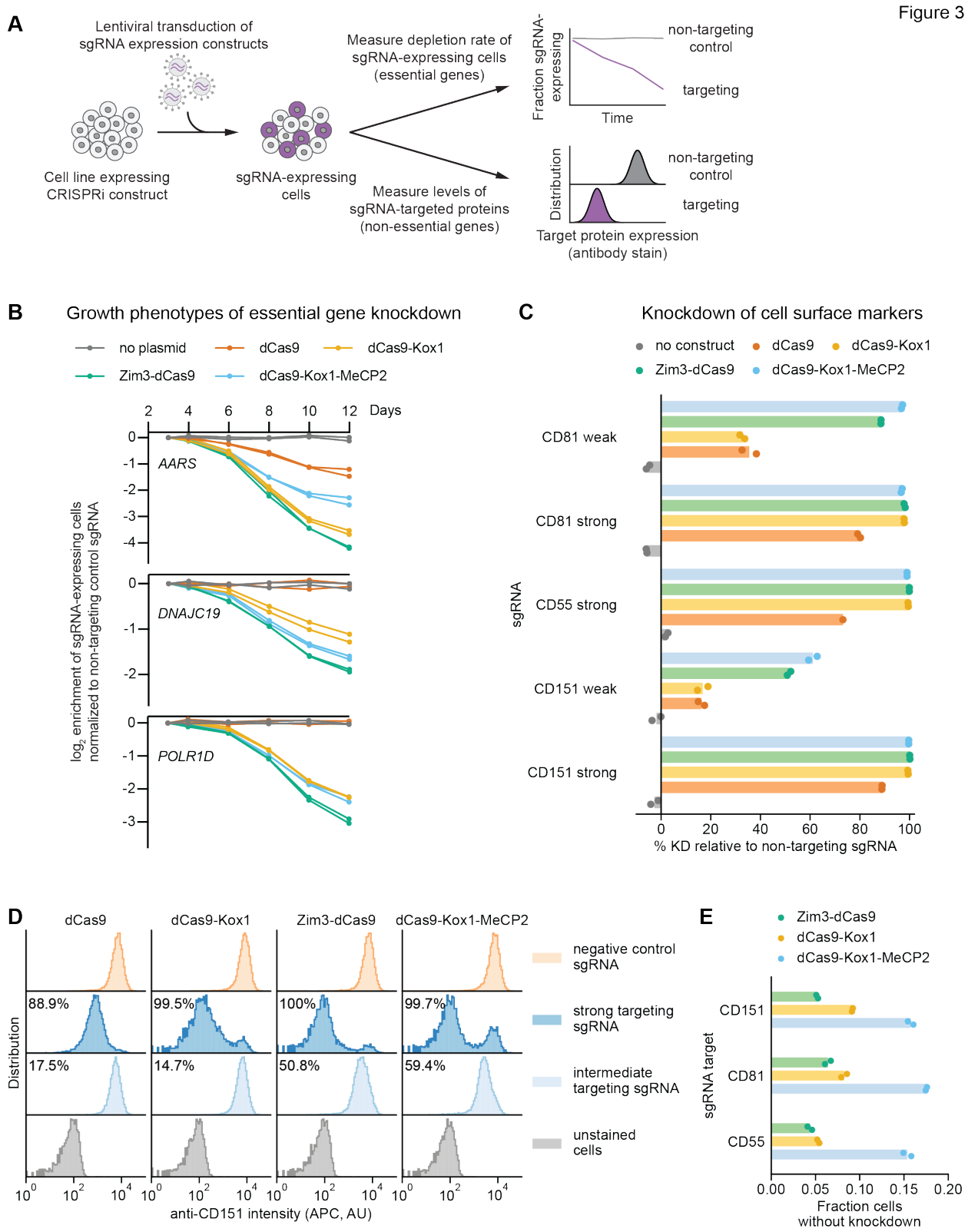

Figure 3. Zim3-dCas9 and dCas9-Kox1-MeCP2 mediate strongest knockdown.

1212 a. Experimental design to measure knockdown mediated by different CRISPRi effectors by
1213 delivering sgRNAs targeting either essential genes or cell surface markers.
1214 b. Depletion of K562 cells expressing essential gene-targeting sgRNAs and different CRISPRi
1215 effectors, measured as the ratio of mCherry-positive (sgRNA-expressing) to mCherry-negative
1216 (not sgRNA-expressing) cells in a given well. mCherry levels were measured for 12 days after
1217 transduction, starting on day 3. Data from two replicate transductions.
1218 c. Percent knockdown of cell surface markers by different CRISPRi effectors in K562 cells. Cell
1219 surface marker levels were measured on day 6 post-transduction by staining with an APC-
1220 conjugated antibody. Knockdown was calculated as the ratio of median APC signal in sgRNA-
1221 expressing cells and median APC signal in cells expressing a non-targeting control sgRNA after
1222 subtraction of background APC signal. Data from two replicate transductions. Cells expressing
1223 dCas9 and a strong CD55-targeting sgRNA are represented by a single replicate.
1224 d. Distribution of anti-CD151 signal intensity (APC) in individual cells from one representative
1225 transduction. Data from second replicate are shown in Figure S3B. Knockdown was quantified
1226 as in Figure 3c.
1227 e. Fraction of cells without observable knockdown despite expressing a strong sgRNA, as
1228 quantified from the fluorescence distributions.
1229
1230 See also Figure S3.

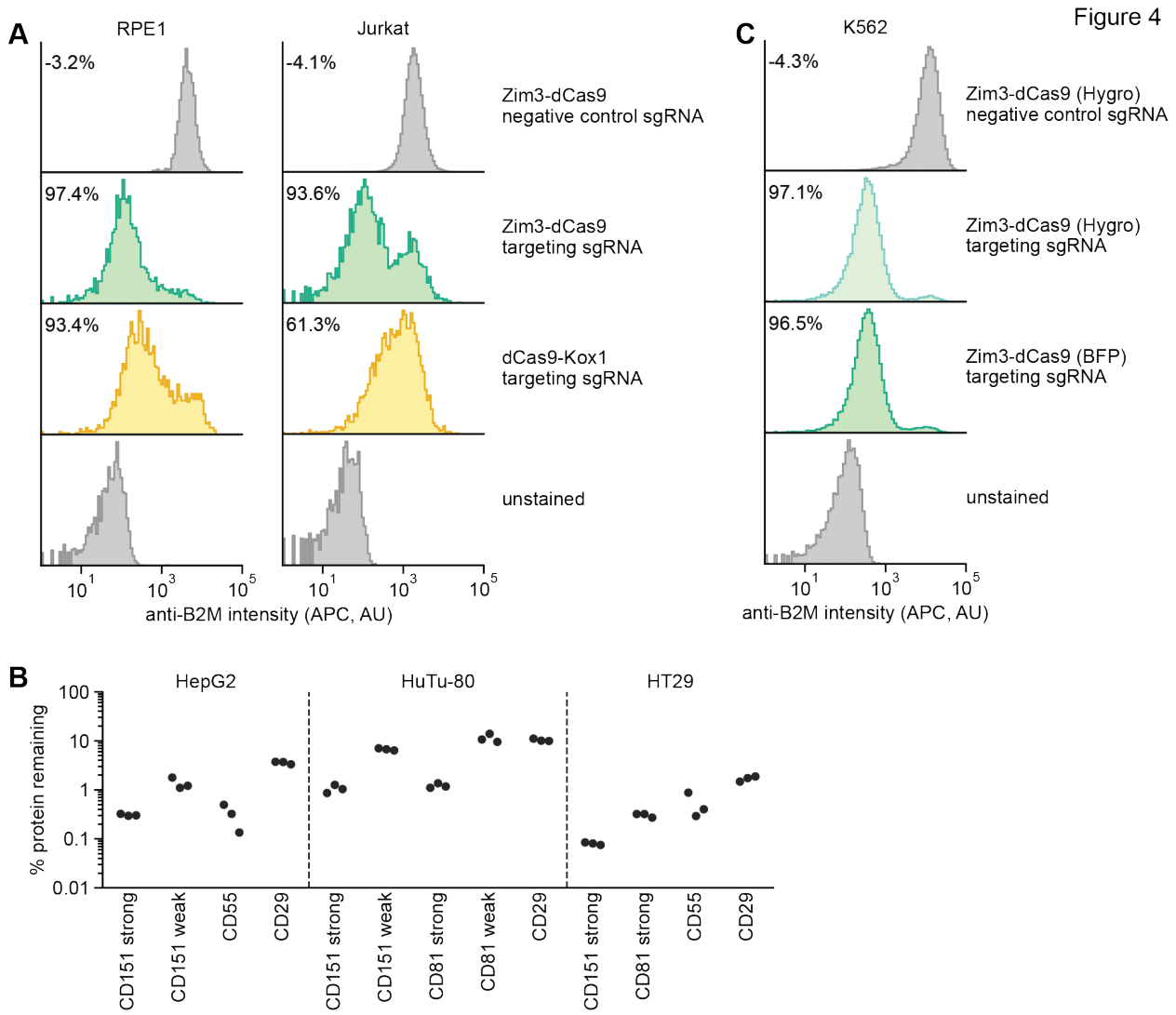

Figure 4. Validation of a suite of optimized Zim3-dCas9 cell lines.

a. Distribution of anti-B2M signal intensity (APC) in individual RPE1 (left) and Jurkat (right) cells expressing indicated CRISPRi effectors and sgRNAs. Knockdown was calculated as the ratio of median APC signal in transduced (sgRNA-expressing) cells and median APC signal in non-transduced cells in the same well, after subtraction of background APC signal.

b. Depletion of indicated cell surface markers in HepG2 (left), HuTu-80 (middle), and HT29 (right) cells expressing Zim3-dCas9. Cell surface marker levels were measured 6-14 days post-transduction by staining with APC-conjugated antibodies. Knockdown was calculated as the ratio of median APC signal in sgRNA-expressing cells and median APC signal in cells expressing a non-targeting control sgRNA after subtraction of background APC signal.

1242 c. Distribution of anti-B2M signal intensity (APC) in individual K562 cells expressing indicated
1243 CRISPRi effectors and sgRNAs. The Zim3-dCas9 (Hygro) cell line was generated by
1244 transduction followed by hygromycin selection and does not express a fluorescent protein.
1245 Knockdown was calculated as in Figure 4a.
1246
1247 See also Figure S4.

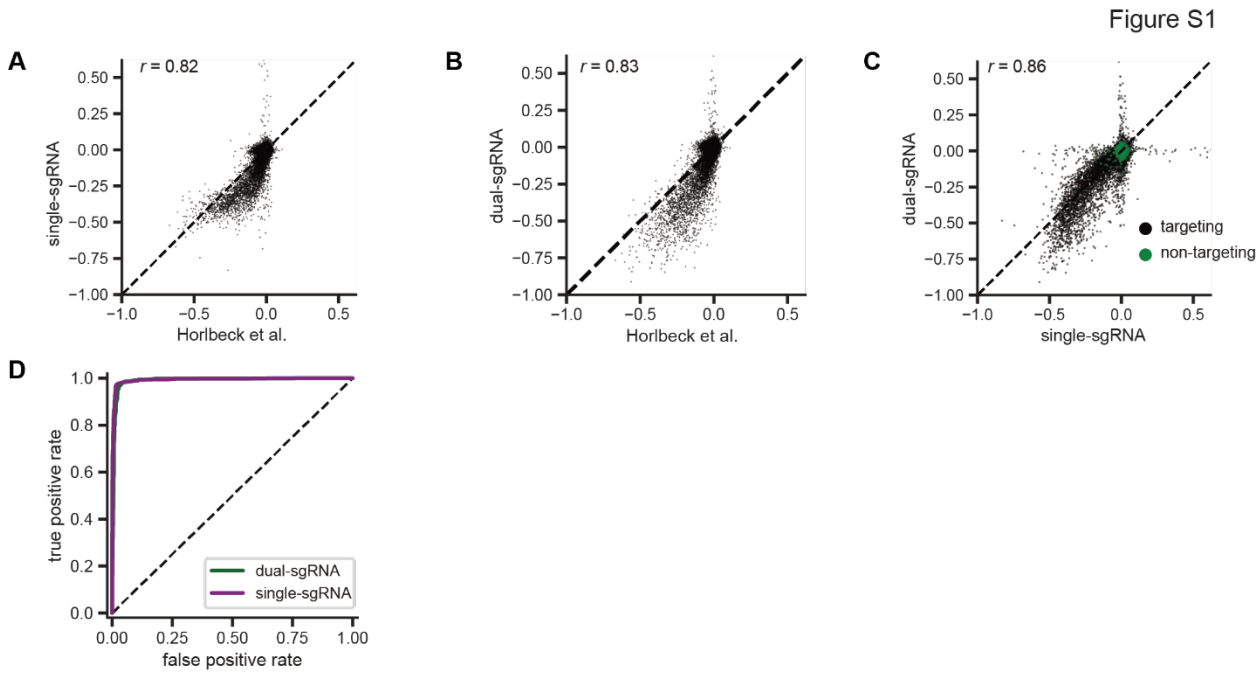

Figure S1. Additional comparisons of pilot single- and dual-sgRNA library screens.

a. Comparison of growth phenotypes for all elements between our pilot single-sgRNA library and Horlbeck *et al.* data, merged by gene name (n=20228 elements). Growth phenotypes are reported as γ ($\log_2$ fold-enrichment of T_{final} over T_0, per doubling) and correlated between experiments (r= 0.82).

b. Comparison of growth phenotypes for all elements between our pilot dual-sgRNA library and Horlbeck et. al data, merged by gene name (n=20228 elements). Growth phenotypes are reported as γ and correlated between experiments (r= 0.83).

c. Comparison of growth phenotypes for all elements between our pilot single- and dual-sgRNA libraries, merged by gene name (n=21239 with 20228 targeting elements and 1011 non-targeting elements). Growth phenotypes are reported as γ and correlated between experiments (r= 0.86).

d. Comparison of true and false positive rates in single element screens. "Positives" (n=1363 elements) were defined as genes with a K562 CRISPRi growth screen p-value < 0.001 and γ < -0.05 (Horlbeck et al., 2016a), and "negatives" were defined as non-targeting control sgRNA pairs (n=1011 elements).

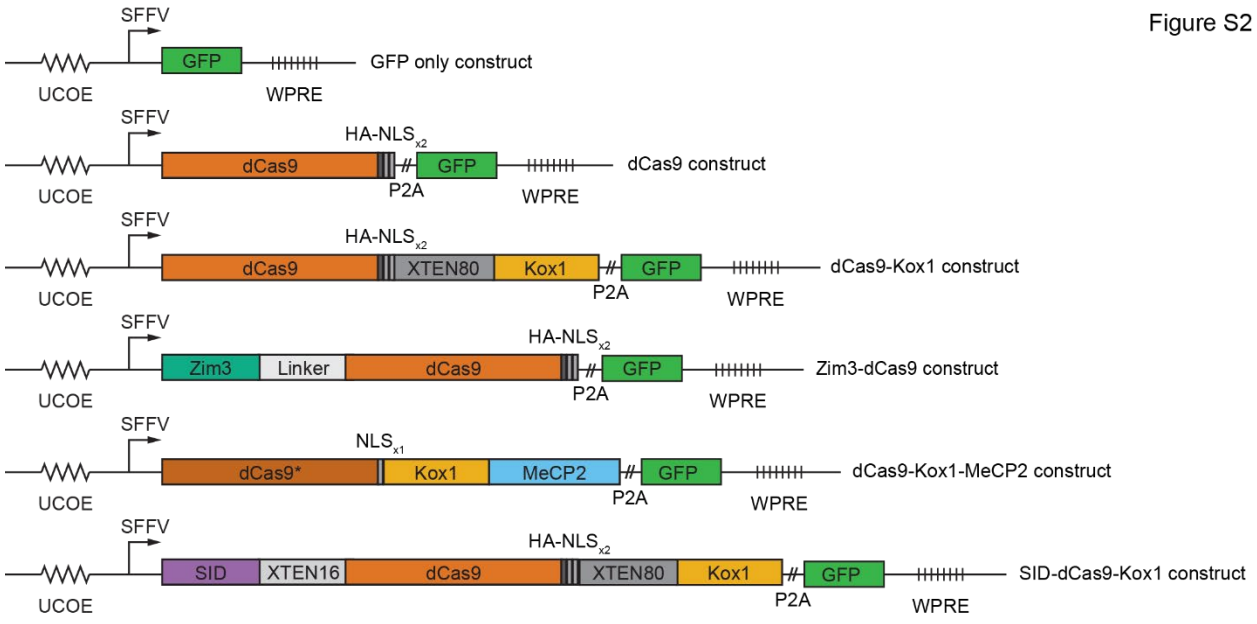

Figure S2. Design of constructs for CRISPRi effector expression.

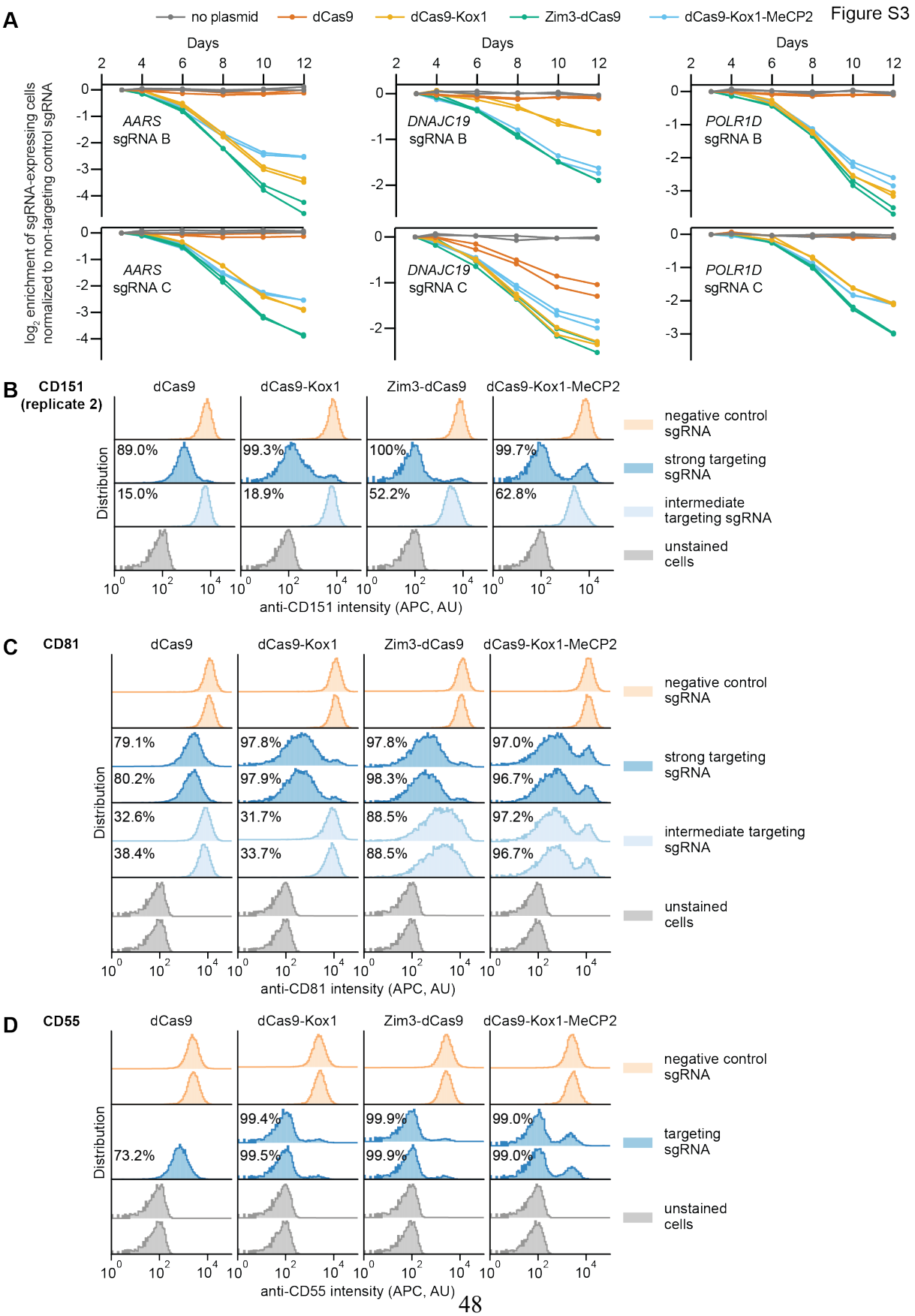
A
no plasmid
dCas9
dCas9-Kox1
Zim3-dCas9
dCas9-Kox1-MeCP2
Figure S3
Days
log2 enrichment of sgRNA-expressing cells normalized to non-targeting control sgRNA
AARS sgRNA B
DNAJC19 sgRNA B
POLR1D sgRNA B
AARS sgRNA C
DNAJC19 sgRNA C
POLR1D sgRNA C
B
CD151 (replicate 2)
dCas9
dCas9-Kox1
Zim3-dCas9
dCas9-Kox1-MeCP2
Distribution
89.0%
99.3%
100%
99.7%
15.0%
18.9%
52.2%
62.8%
negative control sgRNA
strong targeting sgRNA
intermediate targeting sgRNA
unstained cells
anti-CD151 intensity (APC, AU)
C
CD81
79.1%
97.8%
97.8%
97.0%
80.2%
97.9%
98.3%
96.7%
32.6%
31.7%
88.5%
97.2%
38.4%
33.7%
88.5%
96.7%
anti-CD81 intensity (APC, AU)
D
CD55
73.2%
99.4%
99.9%
99.0%
99.5%
99.9%
99.0%
targeting sgRNA
anti-CD55 intensity (APC, AU)

1266

1267 **Figure S3. Additional measurements of on-target activity of CRISPRi effectors.**
1268 a. Depletion of K562 cells expressing essential gene-targeting sgRNAs and different CRISPRi
1269 effectors, measured as the ratio of mCherry-positive (sgRNA-expressing) to mCherry-negative
1270 (not sgRNA-expressing) cells in a given well, as in Figure 3a. mCherry levels were measured for
1271 12 days after transduction, starting on day 3. Data from two replicate transductions.
1272 b. Distribution of anti-CD151 signal intensity (APC) in K562 cells expressing indicated
1273 CRISPRi effectors from second replicate transduction. Knockdown was quantified as in Figure
1274 3c.
1275 c. Distribution of anti-CD81 signal intensity (APC) in K562 cells expressing indicated CRISPRi
1276 effectors from two replicate transductions. Knockdown was quantified as in Figure 3c.
1277 d. Distribution of anti-CD55 signal intensity (APC) in K562 cells expressing indicated CRISPRi
1278 effectors from two replicate transductions. Cells expressing dCas9 and the CD55-targeting
1279 sgRNA are represented by a single replicate. Knockdown was quantified as in Figure 3c.

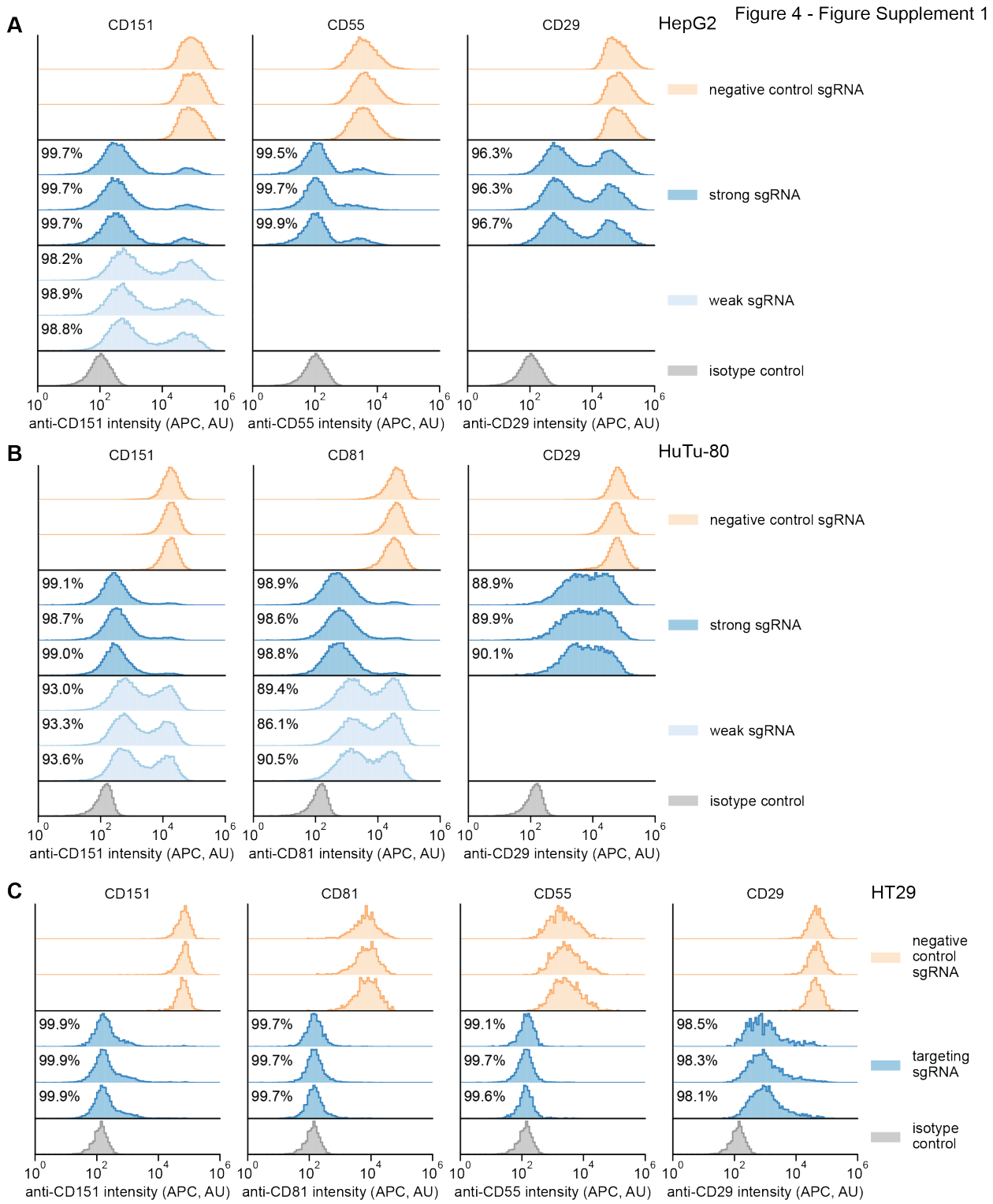

Figure S4. Single-cell distributions of knockdown in different Zim3-dCas9 cell lines. a. Distribution of anti-CD151, anti-CD55, and anti-CD29 signal intensities (APC) in HepG2 cells expressing Zim3-dCas9. Data from 3 independent transductions are shown. A weak

1284 targeting sgRNA was only included for CD151. For the isotype control, cells expressing the
1285 negative control sgRNA were stained with an APC-conjugated isotype control antibody. A single
1286 replicate is shown for the isotype control. Knockdown was calculated as in Figure 4b.
1287 b. Distribution of anti-CD151, anti-CD81, and anti-CD29 signal intensities (APC) in HuTu-80
1288 cells expressing Zim3-dCas9. Data from 3 independent transductions are shown. A weak
1289 targeting sgRNA was only included for CD151 and CD81. For the isotype control, cells
1290 expressing the negative control sgRNA were stained with an APC-conjugated isotype control
1291 antibody. A single replicate is shown for the isotype control. Knockdown was calculated as in
1292 Figure 4b.
1293 c. Distribution of anti-CD151, anti-CD81, anti-CD55, and anti-CD29 signal intensities (APC) in
1294 HT29 cells expressing Zim3-dCas9. Data from 3 independent transductions are shown. Only
1295 strong targeting sgRNAs were included. For the isotype control, cells expressing the negative
1296 control sgRNA were stained with an APC-conjugated isotype control antibody. A single
1297 replicate is shown for the isotype control. Knockdown was calculated as in Figure 4b.

1298 **Supplementary Tables**

1299 Table S1. Dual- and single-sgRNA libraries used for preliminary comparison.

1300 Table S2. Read counts and growth phenotypes from pilot screen.

1301 Table S3. Aggregated CRISPRi sgRNA performance across screens.

1302 Table S4. Finalized dual-sgRNA CRISPRi libraries.

1303 Table S5. List of integration barcodes.

1304 Table S6. Dolcetto versus dual-sgRNA Perturb-seq comparison.

1305 Table S7. Description of plasmids.

1306 Table S8. Sequences of sgRNAs used for individual validation.

1307 Table S9. Dual-sgRNA CRISPRa libraries.

1308

1309 **Supplementary Notes**

1310 Supplementary Note 1. Protocol for cloning dual-sgRNA libraries.

1311 Supplementary Note 2. Protocol for sample preparation and Illumina sequencing of dual-sgRNA

1312 libraries.

1313 Supplementary Note 3. Protocol for arrayed cloning of dual-sgRNA constructs.

1314 Supplementary Note 4. Protocol for generation of CRISPRi cell lines.

1315